



# PVDF-based and its Copolymer-Based Piezoelectric Composites: Preparation Methods and Applications

Xiaofang Zhang<sup>1</sup> · Weimin Xia<sup>1</sup> · Jingjing Liu<sup>2</sup> · Mengjie Zhao<sup>1</sup> · Meng Li<sup>2</sup> · Junhong Xing<sup>3</sup>

Received: 13 December 2021 / Accepted: 8 July 2022 / Published online: 24 July 2022  
© The Minerals, Metals & Materials Society 2022

## Abstract

Recently, for their advantages of lightweight, easy-shaped, good corrosion resistance, biocompatibility, etc., a series of flexible poly (vinylidene fluoride)-based (PVDF-based) piezoelectric composites have been proposed for use in self-powered electronic devices, such as piezoelectric nanogenerators, sensors, wearable electronic units, etc. In this review, we classify the polymer-based piezoelectric composites, combine their preparation method, filler type, structure, and performance, etc., and explain in detail the effects of different preparation methods and filler types on the piezoelectric properties of the composites. Then, the influence of composition, structure, and forming method on the piezoelectric and energy-transforming performances are investigated. Finally, the development trends of these PVDF-based piezoelectric composites are prospected. This review may provide a reference for the academic and application of the polymer-based piezoelectric composites in energy transfer-related and harvesting-related areas.

**Keywords** PVDF · fabrication methods · composite materials · piezoelectric nanogenerators

## Introduction

The increasing demands of environmental protection, low energy consumption, portable, and miniature self-powered electronic equipment require transducers, sensors, and energy-harvesting devices possessing not only the advantages of high electromechanical transferring performance but also the merits of flexibility, light weight, and easy-shaping.<sup>1</sup> As a typical flexible piezoelectric material, polymers show the characters of good chemical stability, high dielectric permittivity ( $\epsilon_r$ ), and high breakdown voltage ( $E_b$ ). However, compared with inorganic ceramics or single crystals, piezoelectric polymers often exhibit a relatively low piezoelectric coefficient which limits the polarization mechanism

of molecular dipoles.<sup>2,3</sup> Thus, in recent decades, to solve this problem and allow the piezoelectric materials to retain their flexible character, many progressive inorganic/polymer piezoelectric composites, consisting of polymer and filler (ceramics or single crystals) phases have been proposed, in which inorganic fillers are often carbon-based materials, metal oxides, and metal particles, and the polymer matrix is mainly comprised of polyvinylidene fluoride (PVDF)-based polymers.<sup>4</sup>

PVDF, as a semi-crystal polymer, is commonly crystallized into four states, the  $\alpha$ -phase,  $\beta$ -phase,  $\gamma$ -phase, and  $\delta$ -phase, among which the  $\beta$ -phase PVDF with a polar crystal structure shows a high piezoelectric property.<sup>5–7</sup> Thus, when using PVDF as the polymer matrix, the key to improving the piezoelectric property of PVDF is to increase the content of the  $\beta$ -phase. Moreover, compared with PVDF, polyvinylidene fluoride-hexafluoropropylene (P(VDF-HFP)) has a relatively high piezoelectric response, a specific relationship of two piezoelectric coefficients,  $d_{31}$  and  $d_{33}$  ( $|d_{31}/d_{33}| > 1$ ), a proper electromechanical coupling coefficient ( $k_{31} = 0.187$ ), and a high Young's modulus.<sup>8,9</sup> The addition of HFP components in the P(VDF-HFP) copolymer greatly improves the mechanical flexibility of the materials.<sup>10</sup> For example, the traditional PVDF film has an elastic modulus of about 2200–2600 MPa, thus it only has an

✉ Weimin Xia  
xiaweimin@xaut.edu.cn

✉ Meng Li  
limeng@xatu.edu.cn

<sup>1</sup> School of Materials Science and Engineering, Xi'an University of Technology, Xi'an 710048, China

<sup>2</sup> School of Materials Science and Chemical Engineering, Xi'an Technological University, Xi'an 710021, China

<sup>3</sup> School of Mechanical and Precise Instrumental Engineering, Xi'an University of Technology, Xi'an 710048, China

inverse piezoelectric coefficient of about 25 pm/V, while the elastic modulus of the copolymer P(VDF-HFP) film is 360~440 MPa, and its inverse piezoelectric coefficient is much higher than that of PVDF.<sup>11</sup> Therefore, by combining P(VDF-HFP) with different functional fillers, it can not only enhance the piezoelectric properties of materials but also improve the mechanical flexibility of the materials, facilitating the preparation of flexible electronic devices.

In addition, binary copolymer polyvinylidene fluoride-trifluoroethylene (P(VDF-TrFE)) were prepared in 1979 by introducing the trifluoroethylene (TrFE) monomer into the VDF chain segment. P(VDF-TrFE) introduces a number of F atoms, whose atomic radius of van der Waals force is greater than that of H atoms. As such, when the content of TrFE exceeds a certain amount, -CHF-CF<sub>2</sub>- and -CH<sub>2</sub>-CF<sub>2</sub>-, the rotation barrier between block polymer TGTC, is formed within the molecular chain structure, which is beneficial for the  $\beta$ -crystal phase.<sup>12,13</sup> Therefore, P(VDF-TrFE) with proper TrFE contents (20–50 mol%) possesses a higher content of the  $\beta$ -crystal that that of PVDF regardless of stretching.<sup>14</sup> Based on this characteristic, P(VDF-TrFE) has attracted considerable attention, and its application scope is increasingly being expanded. Nevertheless, as a polymer, P(VDF-TrFE) has a limited  $d_{33}$  of about -30 pC/N, which is far smaller than that of piezoelectric ceramics.<sup>15</sup>

Recently, electrical energy-harvesting systems, including flexible self-powered electronic devices using piezoelectric

polymers and polymer-based composites as raw materials, have been paid increasing attention, and most of them have been applied in our daily life. We have summarized the recent progress of PVDF-based and its copolymer-based self-powered electronics as illustrated in Fig. 1, which include relevant energy-harvesting applications in different fields.<sup>16–20</sup> For example, based on the advantages of good flexibility, light weight, and easy processing of PVDF and its copolymers, fabricated self-powered electrical equipment can act on any irregular object, and be used to sense various forms of external forces,<sup>21</sup> such as human motion, wind energy, vehicle movement, etc. In addition, these polymers can be used to make wearable electronics or clothing, and are even expected to be used in aerospace and sports in the future. Therefore, optimizing self-powered electronics based on PVDF and its copolymers for higher sensitivity and greater output power, thus laying the foundation for a variety of applications such as wearable devices, implant fields, industrial environments, etc., is an ongoing goal for researchers.

To compound the inorganic fillers into polymer matrix, it is still necessary to consider the effects of different preparation processes on the defects and losses of materials, as well as the orientation effect of processing methods on the filler. A reliable preparation method can improve the compatibility between the polymer matrix and the filler, reduce the interface defects, and thus achieve the purpose of effectively

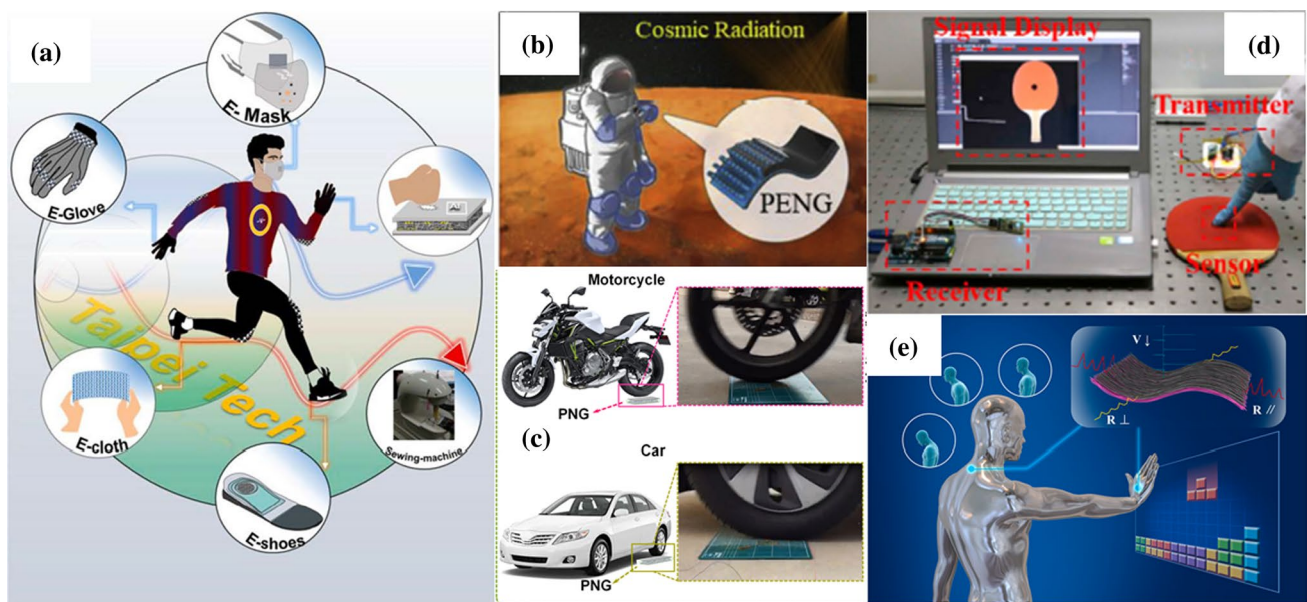


**Fig. 1** (a) Scheme of energy harvesting performance in distinct methods. (Adapted with permission from Ref. 16, copyright Elsevier). (b) Schematic of a piezoelectric nanogenerator (PENG) application for space energy harvesting. (Adapted with permission from Ref. 17, copyright Elsevier). (c) Schematic and photographic images of the corresponding vehicles passing on a Ag/BTO-PNG device. (Adapted

with permission from Ref. 18, copyright Elsevier). (d) A wireless system presenting the function of locating the ball. (Adapted with permission from Ref. 19, copyright Elsevier). (e) Schematic of a multi-functional sensor and its potential applications. (Adapted with permission from Ref. 20, copyright Elsevier).

enhancing the piezoelectric properties of polymer-based composites. In this review, we will provide the different types of filler doping and different preparation methods for the preparation of PVDF, P(VDF-HFP), P(VDF-TrFE), and other PVDF copolymer-based piezoelectric composites. Then, the use of different preparation methods of polymer-based piezoelectric composite materials is presented, and the prospects of applications in the future will be discussed. This work is expected to provide a help and guidance for further research on PVDF-based piezoelectric composites.

## Fabrication Methods of Polymer-Based Piezoelectric Composites

Although the piezoelectric properties of the PVDF-based composites can be improved by the addition of highly polar inorganic fillers, the influencing mechanisms are not very clear. Moreover, the piezoelectric properties of the materials are closely related to the preparation method, which is used to design the structure of these composites. The main preparation methods of these polymer-based piezoelectric composites include electrospinning, solution-casting, spin-coating, hot-pressing, tape casting, etc.

### Electrospinning

Electrospinning is a special fiber manufacturing method, referring to a process of a polymer solution forming nanoscale fibers under the action of a high-voltage electrostatic field.<sup>22,23</sup> Under a high voltage, the spinning liquid droplets or melt will be changed from spherical to cone-shaped (that is, a “Taylor cone”), and a continuous increase of the electric field force will charge the droplets and eventually form a cone. Then, the cone indicates the surface tension of the jet and continues to be stretched, refined, and solidified through solvent evaporation. Finally, a non-woven fabric falls on the receiver. Electrospinning has many advantages, such as simple electrospinning equipment, ease of operating, controllable spinning process, and relatively low cost. Moreover, electrospinning is performed in an electric field environment, and this process combines mechanical stretching and electrical polarization,<sup>24</sup> which is conducive to the formation of  $\beta$ -phase PVDF.<sup>25</sup> Therefore, the PVDF-based composite film prepared by electrospinning can be directly treated as a piezoelectric film.<sup>26</sup> 3D multilayer nanofiber mats (NFMs) have been designed and prepared using both electrospinning and electrospraying, in which piezoelectric PVDF nanofibers are the piezoelectric layer, PPy/PVDF nanofibers the upper and lower electrode layers, and CsPbBr<sub>3</sub>@PVDF bead particles the piezoelectric layer,<sup>27</sup> as illustrated in Fig. 2. Compared with that of piezoelectric nanogenerators (PENGs) based on ordinary

three-layer PVDF nanofibers (piezoelectric PVDF nanofiber and ppy/PVDF nanofiber), the piezoelectric output voltage of 3D multilayer NFMs increased from 6.79 V to 10.3 V, and the current density was enhanced from 0.88  $\mu\text{A}/\text{cm}^2$  to 1.29  $\mu\text{A}/\text{cm}^2$ . It is believed that the introduction of CsPbBr<sub>3</sub>@PVDF microbeads into NFMs can effectively transfer the applied stress and promote the stress excitation of piezoelectric nanogenerator piezoelectric layer, and thus improve the output performance.<sup>28</sup> However, there are some problems in the process of preparing piezoelectric films by electrospinning, as the internal fibers of polymer-based piezoelectric composites prepared by electrospinning may have a chaotic arrangement, which will produce mutually canceling effects, so that the overall piezoelectric properties of the film will be reduced.

### Spin-Coating

Spin-coating is the preferred method for obtaining thin and uniform films on flat substrates.<sup>29–32</sup> Filler/polymer mixed solution droplets are spun on a horizontal rotary table rotating at a certain rotation speed, resulting in the projecting and evaporation of the solution, forming solid films. Compared with the preparation of composite membranes by a variety of methods, spin-coating has many advantages, such as precision control of the thin film thickness, energy saving, low pollution, with no stretching or hot polarization during the post-processing step.<sup>33</sup> In the process of spin-coating, the composite film is sheared, equivalent to the role of mechanical drawing. Moreover, it undertakes orientations that induce polymer molecular chains, promotes the formation of the  $\beta$ -phase, and improves the piezoelectric properties. Therefore, spin-coating has a broad application prospect in microelectronics technology, nanophotonics, biology, medicine, and other fields. A strategy of preparing different composite layers to achieve synergistic effects has been reported. Figure 3 shows a double-layer (DL) PVDF-based nanocomposite, preparing by spin-coating, which is composed of a layer of barium titanate (BaTiO<sub>3</sub>) nanoparticles (NPs), forming a BT NPs/PVDF layer, and a pure PVDF layer.<sup>34</sup> As a comparison, pure PVDF monolayer (SL) films of a similar thickness and content were also prepared. The results show that the piezoelectric output of the PENGs made of DL nanocomposite film is greater than that of the piezoelectric output of the PENGs made of SL nanocomposite film. When the BT NPs content was 20 vol%, the DL film exhibited an excellent comprehensive performance of an output voltage of 6.7 V and an output current of 2.4 A, and showed good ductility and output stability. However, some parameters in the spinning process will affect the performance of the composite film and, therefore, it is necessary for the film preparation to be continuously optimized.<sup>35</sup>

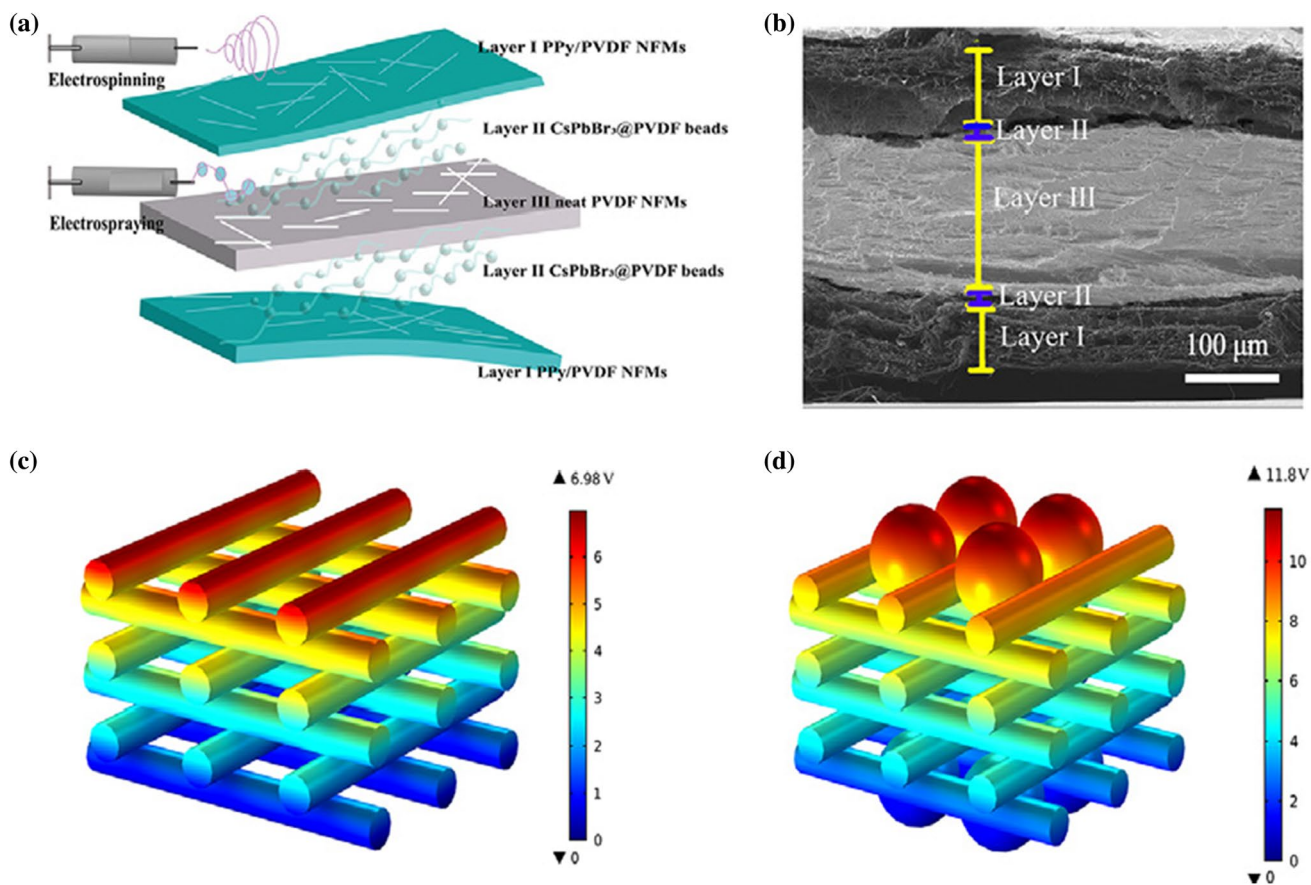


**Fig. 2** (a) Schematic of 3D multilayer NFMs constructed by PPy/PVDF NFMs (*Layer I*), CsPbBr<sub>3</sub>@PVDF beads (*Layer II*) and neat PVDF NFMs (*Layer III*), respectively. (b) Cross-section scanning electron microscope image of 3D multilayer NFMs. (c, d) Simulation

piezoelectric responses of (c) the three-layer NFMs and (d) 3D multilayer NFMs at an applied pressure of 6 kPa. (Adapted with permission from Ref. 27, copyright Elsevier).

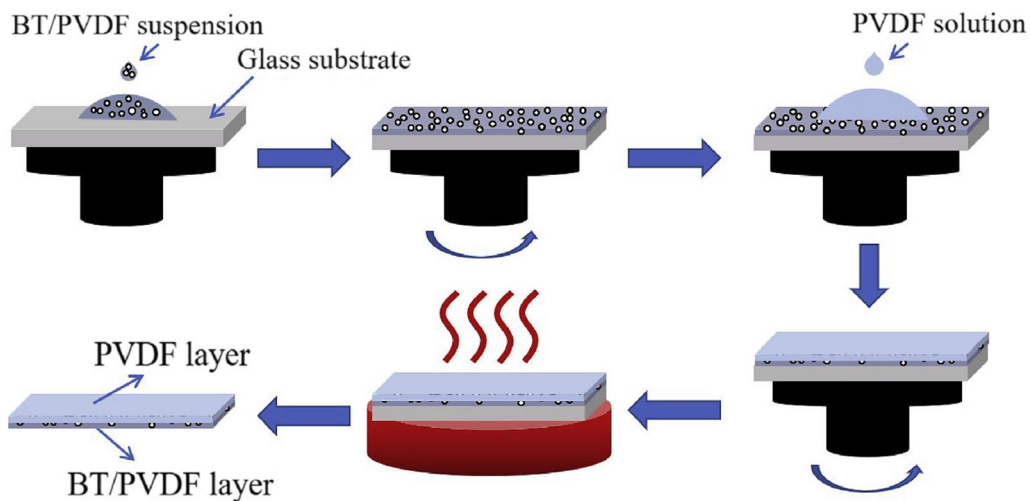


**Fig. 3** Schematic of the solution spin-coating process of the double-layered BT/PVDF nanocomposite films. (Adapted with permission from Ref. 34, copyright Elsevier).

## Solution-Casting

Solution-casting, as a preparation method of filler/polymer composites, selects a polymer and a filler according to certain proportions and joins a specific percentage of solvent in the filler/polymer mixed solution.<sup>36–38</sup> By making a dissolved mixture at a certain temperature, a dispersed filler/polymer mixed solution is obtained and placed in a vacuum drying oven. After the solvent has completely evaporated, a composite film is obtained from the casting solution on a clean substrate. Compared with other methods, the preparation process is simpler and more convenient. Therefore, the preparation of filler/polymer composites by solution-casting has been commonly applied. For example, Wegener et al. prepared a composite film of lead zirconate titanate (PZT) and P(VDF-HFP) with a thickness of 100  $\mu\text{m}$  by solution-casting.<sup>39</sup> Within the 0–3 composites, the ceramic volume fraction was varied between 0.19 and 0.65, which yielded films with different structural and dielectric properties. These influenced the piezoelectric properties of the composite films found after electric poling, which was performed at room temperature. The polarization experiments under corona discharge and direct contact show that the polarization of ceramic particles is the main source of piezoelectric activity in the direction of ceramic film thickness, and the maximum  $d_{33}$  is 11 pC/N (actually  $d_{33}$  should be a negative value). Although the process of solution-casting is simple and easy to operate, and the requirements for experimental equipment are not very high, the thickness of the film prepared by this method is not easy to control, resulting in a poor thickness uniformity of the film. Therefore, it is only suitable for products with low requirements for film thickness. In addition, most of PVDF-based films produced by solution-casting are of the  $\alpha$ -PVDF crystal type, which has little piezoelectric property. In order to improve the piezoelectric properties, the prepared film needs to be further treated, such as high-electric field polarization,<sup>40</sup> stretching,<sup>41</sup> etc., to make it have a larger  $\beta$ -crystal phase proportion.

## Hot-Pressing

In the process of hot-pressing, a certain amount of filler and polymer is first prepared, with the functional filler evenly dispersed in the polymer matrix by solution- or melt-blending. After heating the compounds to reach the melting point of the polymer, it is hot-pressed into a designed shape, and the piezoelectric composite is obtained after slow cooling. Many researchers have adopted hot-pressing to prepare composite materials, due to its advantages, such as not needing to prepare slurry and its relatively simple process.<sup>42–44</sup> PZT/PVDF composite materials by hot- and cold-pressing were prepared, and the influence of different preparation

processes on the structure and electrical properties of PZT/PVDF piezoelectric composite materials were investigated.<sup>45</sup> It was found that the PZT/PVDF composite prepared by hot-pressing has better electrical performance than that prepared by cold-pressing, and that the PZT/PVDF composite prepared by hot-pressing is compact, and has the characters of a high dielectric constant and low dielectric loss. The main reason is that the preparation process of hot-pressing can significantly reduce interface defects between the ceramic and polymer phases and depress the porosity of the composites. Recently, a textured flexible piezoelectric composite with excellent service characteristics of polar nanorods was developed by hot-pressing.<sup>46</sup> In order to obtain the best energy-harvesting performance in the cantilever mode, oriented  $\text{BaTi}_2\text{O}_5$  nanorods (BT2) were arranged horizontally in the polymer matrix, so that they could adapt to the stress orientation and undergo sufficient deformation. As a result, under the guidance of design theory of molten salt synthesis with single-axle strong polarity of BT2 as the filler, PVDF as the matrix, and by the hot-pressing orientation process with BT2 in the polymer matrix orientation, energy-harvesting BT2/PVDF piezoelectric composites were constructed with a high transfer coefficient, as shown in Fig. 4. It was found that the cantilever-type flexible piezoelectric energy scavenger exhibited a high energy density of 27.4  $\mu\text{W}/\text{cm}^3$  under severe vibration conditions (10 g acceleration). More importantly, after a long period of vibration cycles ( $\sim 330,000$ ), the flexible piezoelectric energy scavenger could maintain its power generation characteristics without deterioration.

Although the hot-pressing is widely used for its many advantages, it is still difficult to control the distribution of the filler phase in the powder mixing process, so that the filler phase is seriously agglomerated. Thus, the interface between the filler phase and the polymer phase is poor, and the high porosity of the composite material has negative influences on its piezoelectric property. In addition, the electrical properties of the piezoelectric composites prepared by hot-pressing are affected by the temperature and pressure during the preparation process. When the hot-pressing temperature is too high, defects inside the materials will occur and the samples are not easy to be polarized, which reduces the piezoelectric properties of the piezoelectric composites,<sup>47</sup> and thus the thermal pressure and temperature should be strictly controlled.

## Other Preparation Methods

In addition to the main preparation methods mentioned above, there are many other preparation methods for different purposes, such as cold-pressing,<sup>48</sup> in situ polymerization, blade-casting,<sup>49,50</sup> tape-calendering,<sup>51,52</sup> low-temperature hydrothermal,<sup>53</sup> melt-blending,<sup>54</sup> solvent evaporation,<sup>55</sup> double-helix melting spinning, and so on.<sup>56</sup> A composite

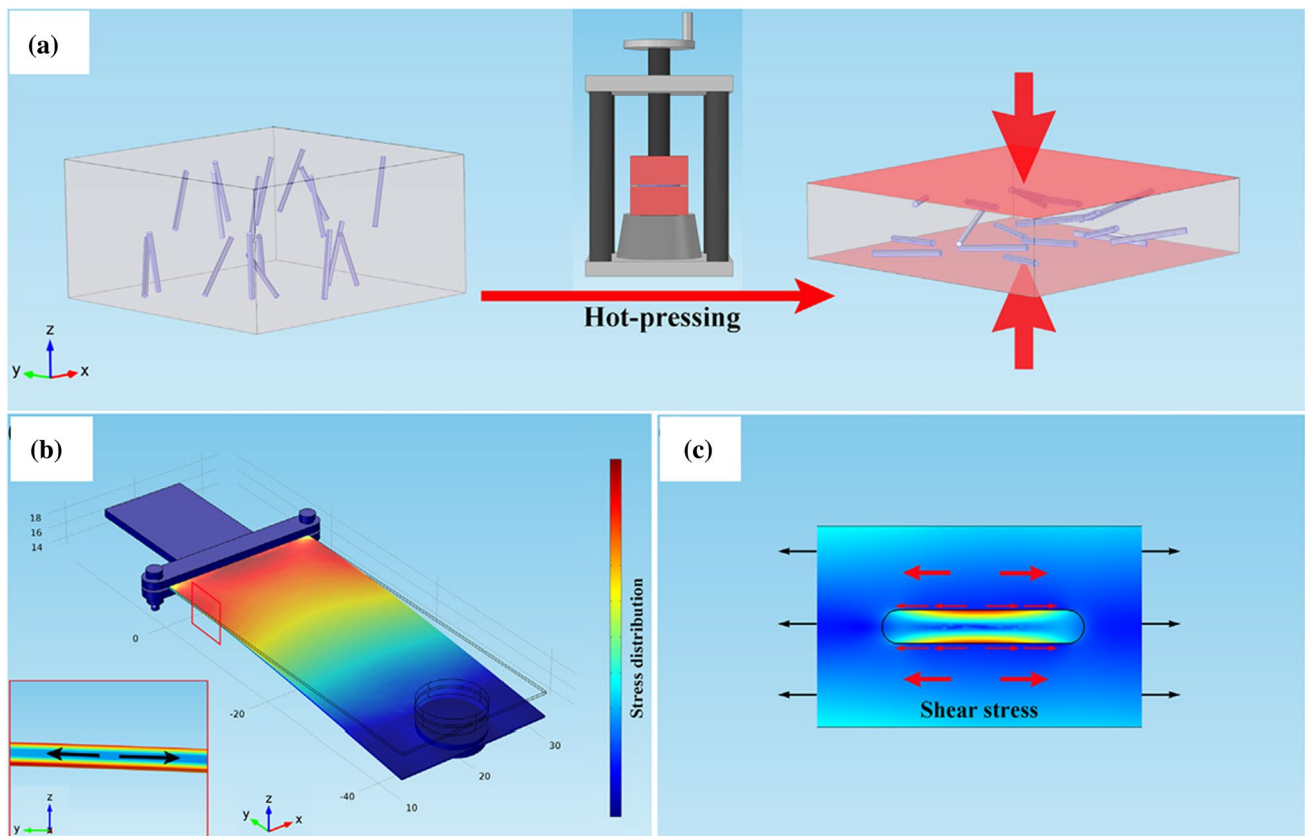


**Fig. 4** (a) Schematic of the hot-pressing process for building a textured BT2/PVDF composite. (b) Schematic of cantilever beam vibration and force analysis results. (c) Spatial distribution of the stress

along the load direction of a single BT2 nanorod. (Adapted with permission from Ref. 46, copyright Elsevier).

with enhanced hydrophilicity was prepared by adding  $\text{TiO}_2$  or  $\text{SiO}_2$  nanoparticles during the in situ polymerization of methyl methacrylate (MMA) in PVDF.<sup>57</sup> The in situ polymerization method could evenly disperse  $\text{TiO}_2$  and  $\text{SiO}_2$  into a PVDF matrix and provide strong interface effects in  $\text{TiO}_2$ /poly(methyl methacrylate) (PMMA)/PVDF and  $\text{SiO}_2$ /PMMA/PVDF samples. The results showed that the  $\text{TiO}_2$ /PMMA/PVDF composites with  $\text{TiO}_2$  content (0~5 wt%), and PVDF matrix in the  $\beta$ -phase content increased from 19 to 43%, and exhibited enhanced piezoelectric performance. Moreover, in the  $\text{SiO}_2$ /PMMA/PVDF composites with  $\text{SiO}_2$  content (0~5 wt%), the  $\beta$ -phase content showed almost no change even with the addition of  $\text{SiO}_2$ , and, therefore, the piezoelectric performance of this composite did not improve. Zhou et al. proposed a PENG based on BT NPs, P(VDF-TrFE), and a silver flake-based electrode by using an all-3D printable process suited for additive manufacturing.<sup>58</sup> The introduction of PENGs can make any design of rapid prototyping in the shape of complex three-dimensional structures, which have low cost and high efficiency. Also, the process can eliminate cutting and subsequent steps, such as mould manufacturing. Figure 5 shows the printing and polarization

process of this piezoelectric device. Because the PENG has excellent tensile properties, the maximum open-circuit voltage ( $V_{oc}$ ) was 6 V and short-circuit current was  $2 \mu\text{A}/\text{cm}^2$ , and it can withstand large strains up to 300%.

In order to explore a new preparation method for preparing high-performance composites, researchers have tried combining two or more methods to prepare composite materials. For example, Guan et al. used polydopamine (Pdp)-modified BT NPs (Pdp-BT) and P(VDF-TrFE) to prepare Pdp-BT/P(VDF-TrFE) composite films by using the ultrasonic process and electrospinning to fix Pdp-BT on the surface of P(VDF-TrFE) nanofibers.<sup>59</sup> Figure 6 shows the preparation process of a P(VDF-TrFE) fiber network. Pdp-BT nanoparticles were fixed on the P(VDF-TrFE) fiber network. The process of ultrasonic stirring will produce the bursting of bubbles and shock waves with a microjet, and the Pdp-BT nanoparticles distribute to the nanometer fiber membrane surface at a very fast speed, where the two interfaces collide, softening the polymer nanofibers, and the nanoparticles attach to the surface of the nanofibers. This preparation method can not only effectively avoid the agglomeration of nanofillers in the polymer matrix but also

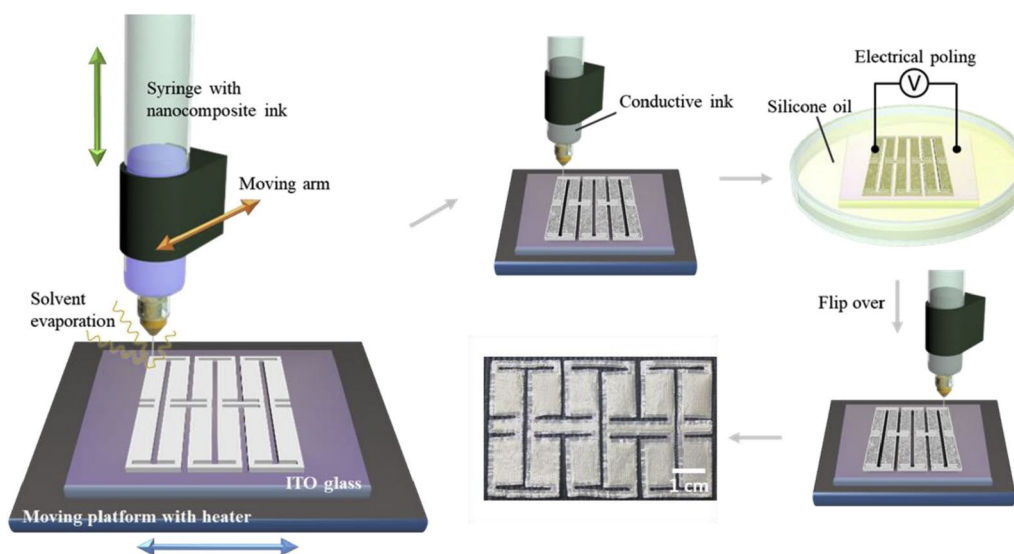


Fig. 5 Schematic of the fabrication process of a 3D-printed PENG.<sup>58</sup>

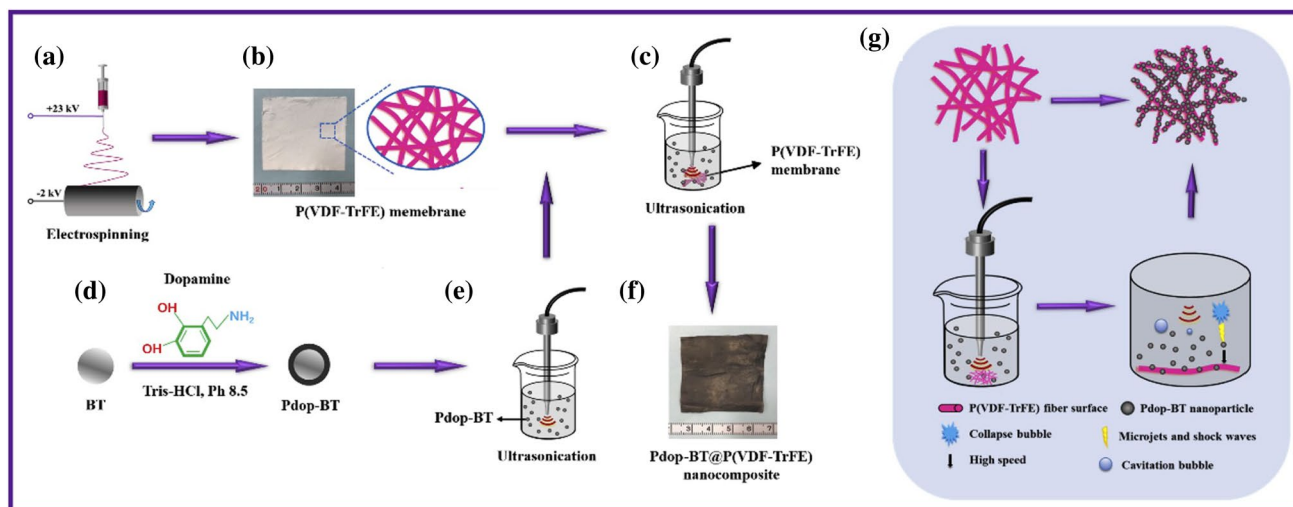


Fig. 6 Schematic of the preparation of Pdp-BT/P(VDF-TrFE) nanocomposites. (a) Schematic of the electrospinning process. (b) Digital image of the as-electrospun mat (*inset* illustration of P(VDF-TrFE) network). (c) Schematic of preparation of Pdp-BT. (d) Preparation of Pdp-BT dispersion with ultrasonication. (e) Pdp-BT decoration

using ultrasonic treatment. (f) Digital image of Pdp-BT/P(VDF-TrFE) nanocomposite. (g) Schematic of Pdp-BT nanoparticles-anchored P(VDF-TrFE) fibrous network. (Adapted with permission from Ref. 59, copyright Elsevier).

enhance the interface density of nanocomposites, and thus the output performance is significantly improved. Compared with PENG-based pure electrospun P(VDF-TrFE) and BT/P(VDF-TrFE), the piezoelectric performance of PENGs prepared by Pdp-BT/P(VDF-TrFE) nanocomposite mats is significantly improved. In addition, the output voltage and current of Pdp-BT/P(VDF-TrFE)-based PENGs can reach  $\sim 6$  V and  $\sim 1.5$   $\mu$ A, which are 4.8 times and 2.5 times, respectively, those of PENG-based pure P(VDF-TrFE). Similarly, Zhang et al. prepared PVDF/PZT piezoelectric films by extrusion-casting and solvent-casting, and investigated

the mechanical, dielectric, ferroelectric, and piezoelectric properties, as well as the breakdown strength of the PVDF/PZT films.<sup>60</sup>

As discussed above, the piezoelectric properties of polymer-based piezoelectric composites are closely related to the preparation method. When the functional filler is combined with the polymer matrix, different preparation methods have different effects on the piezoelectric properties of the composites. For PVDF, electrospinning is preferred, because the electrospinning of PVDF nanofiber composite materials is usually better than solution-casting or cold-pressing.

Moreover, the electrospinning is carried out for the polarization and stretching of composite nanofibers, and revokes the redundant steps of secondary polarization. Therefore, electrospinning has become a preferred method to develop the electroactivity of PVDF-based piezoelectric composites.

Furthermore, for P(VDF-TrFE)-based piezoelectric composite materials, the TrFE introduction in P(VDF-TrFE) will hinder the free rotation and arrangement of VDF chains, and makes part of the VDF molecular chain arrangement change into a trans-structure, which is conducive to the formation of the  $\beta$ -phase. Therefore, P(VDF-TrFE) films with suitable TrFE content favors a high  $\beta$ -crystal content; that is, the stretching step such as in electrospinning is not required. Meanwhile, among the various preparation methods of P(VDF-TrFE)-based piezoelectric composites, solution-casting is the most selected.

## Functional Fillers

### Ferroelectric Ceramics

Piezoelectric ceramics, such as PZT,<sup>61</sup> BT, and potassium sodium niobate (KNN),<sup>62,63</sup> have the advantages of excellent piezoelectric properties, low dielectric loss, high electromechanical coupling coefficients, and high dielectric constants. According to the effective medium theory,<sup>64</sup> the introduction of ceramic fillers with high dielectric constants and large  $d_{33}$  into the polymer matrix is beneficial for improving the electrical properties of the composites.<sup>65–68</sup> Ponraj et al. prepared KNN/PVDF composites by embedding PVDF with KNN powders of different grain sizes (nano-sized and micron-sized) using hot-pressing.<sup>69</sup> They found that, when the nano-sized and micron-sized KNN fillers exceed 10 vol% in the PVDF, the added KNN filler can promote the formation of the polar  $\beta$ -phase, and especially when the nano-sized KNN is added. As such, PVDF-based composites with 70 vol% KNN (micron grain size) has a higher  $d_{33}$  of 35 pC/N. An et al. prepared P(VDF-TrFE)-based composite nanofibers embedded with barium strontium titanate (BaSrTiO<sub>3</sub>) nanoparticles by electrospinning, and further prepared PENGs for water wave energy harvesting.<sup>70</sup> The sustainability of the PENG was improved by the addition of the BaSrTiO<sub>3</sub> nanoparticles in the P(VDF-TrFE) nanofibers by enhancing their ferroelectric properties. Compared with previously reported PENGs, these samples show a superior durability in terms of mechanical properties and cyclability. A high output voltage of 8–12 V was obtained at a pressure of 10 kPa lower than finger pressure. Singh et al. used sodium metaniobate (NaNbO<sub>3</sub>), graphene oxide (RGO), and PVDF to synthesizing flexible NaNbO<sub>3</sub>/RGO/PVDF nanocomposite films by solution-casting and explored its application in nanogenerators.<sup>71</sup> It was found that the output voltage of

nanogenerator-based NaNbO<sub>3</sub>/RGO/PVDF nanocomposite films is ~2.16 V, and the short-circuit current reached 0.383 mA. In this composite, NaNbO<sub>3</sub> nanorods contribute to the arrangement of electric dipoles in the PVDF, and improve the overall piezoelectric properties of the composite film due to their inherent piezoelectric properties. Simultaneously, the presence of RGO helps to move the charge generated inside the film, and further allows PVDF dipole alignment, which favors an enhanced piezoelectric response.

In addition to PVDF, composites comprised of ceramics and P(VDF-TrFE), P(VDF-HFP), and P(VDF-CTFE) have been commonly investigated. The research on the composite materials based on these copolymers has mainly focused on their dielectric and energy storage properties rather than on their piezoelectric properties. Kang et al. prepared a 0–3 PZT/P(VDF-TrFE) piezoelectric composite film with a weight ratio of 85/15 by using a hot-rolling mill and corona discharge, and, following that, developed an acoustic emission sensor based on the piezoelectric composite film.<sup>72</sup> The  $d_{33}$  of PZT/P(VDF-TrFE) was 34.0 pC/N, and the static piezoelectric strain constant ( $d_{31}$ ) was 18.1, which exhibited a fast response and a high sensitivity, and so can be used in acoustic emission sensors. Choi et al. prepared PZT/P(VDF-CTFE) composites by hot-pressing,<sup>73</sup> and found that, although the volume fraction of ceramics added in previous studies was similar, the values obtained were much higher than those in the other studies, as shown in Table I. Especially, when the volume fraction was 70 vol%, the  $d_{33}$  of the piezoelectric composite reached its maximum value of 93 pC/N.

### Metal Oxides

Because metal oxides have a large specific surface area, it is easy to produce interface polarization with a polymer. Metal oxide-doped polymer matrix composites have achieved improved piezoelectric properties. The main reason is that

**Table I** Ceramic volume fraction, permittivity, and piezoelectric properties of piezoelectric ceramic-polymer composites<sup>73</sup>

Material	Volume (vol%)	Permittivity $\epsilon_r$	$d_{33}$ (pC/N)	$d_{33} \times g_{33}$ (pm <sup>2</sup> /N)
PZT-P(VDF-CTFE)	50	80	53	3.98
	60	118	87	7.27
	70	149	92	6.44
PZT-polyester resin	65	88	29	1.08
PZT-PVDF	65	45	33	2.73
PZT-P(VDF-HFP)	48	62.6	11.3	0.23
PMN-PT-P(VDF-TrFE)	40	37.3	31	2.91

$g_{33}$  and  $d_{33} \times g_{33}$  stand for the piezoelectric voltage constant and figure-of-merit, respectively



metal oxides can serve as  $\beta$ -phase crystallization of a polymer matrix or as a nucleating agent, and promote the formation of the  $\beta$ -phase. The commonly used metal oxides are ZnO, TiO<sub>2</sub>, etc. Among them, ZnO is a direct band gap II–VI semiconductor, which has the advantages of high-temperature and high-pressure resistance, abundant sources of low noise materials, and low price. As a typical piezoelectric material with an asymmetric crystal structure, ZnO has a strong spontaneous polarization,<sup>74</sup> and the films made from it also have good piezoelectric properties.<sup>75–79</sup> Phoo-plub et al. prepared ZnO/P(VDF-HFP) composites by combining the polymer P(VDF-HFP) with different forms of ZnO, i.e., nanoparticles (NPs), nanorods (NRs), and microrods (MRs), using solution-casting.<sup>80</sup> Table II summarizes the material properties of ZnO NPs, ZnO NRs, and ZnO MRs with different additions. Compared with ZnO NPs, polymer matrix composite films containing ZnO NRs and ZnO MRs have a higher crystalline phase and a higher elastic modulus. For ZnO NPs and ZnO NRs, when the addition of ZnO is 2 wt%, the electroactive phase of the polymer matrix film is significantly enhanced. When the cantilever vibration is 32 Hz, the composite doped with 2 wt% ZnO NRs has the best open-circuit voltage output and energy-harvesting performance, and can harvest mechanical energy at a lower vibration level. Karumuthil et al. prepared a P(VDF-TrFE)/ZnO NPs and exfoliated graphene oxide (edcx) composite by solution-casting used it as the friction piezoelectric layer of an energy-harvesting device,<sup>81</sup> and they found that the maximum output voltage and current of the prepared device were 2.27 V and 9 nA, respectively, using the finger-tapping test.

## Carbon-Based Materials

Recently, for their specific electronic transport and surface structure characters, carbon-based materials RGO, graphene oxide (GO), carbon nanofibers (CNFs), carbon nanotubes

(CNTs), graphene (Gr), carbon black (CB), etc., have shown great application value in improving the piezoelectric properties of PVDF-based piezoelectric composites. RGO, CNTs, and CB are typical low-dimensional carbon-based materials, and the  $sp^2$  hybridization of the carbon atoms that make up Gr gives it the high carrier mobility and conductivity. In the preparation process of Gr, a large number of defects and groups are introduced, which destroys the complete lattice structure of the Gr, leading to the redistribution of electrons, and making many positive and negative charge centers gather to form dipoles and polarization enhancement. In this material, the large specific surface area is more conducive to the construction of conductive networks and can reduce the internal resistance, which is conducive to PENGs, and so obtain a better piezoelectric output performance. RGO has abundant defects and groups as polarization centers,<sup>82</sup> which increases the polarization. CB has a very large surface area and can promote  $\beta$ -nucleation during the preparation of polymer matrix composites. Moreover, some other carbon-based materials have been selected as fillers.<sup>83–86</sup>

Anand et al. prepared PVDF, RGO/PVDF, Bi<sub>2</sub>Al<sub>4</sub>O<sub>9</sub>/PVDF, and Bi<sub>2</sub>Al<sub>4</sub>O<sub>9</sub>/RGO/PVDF nanocomposites by solution-casting, and investigated the effects of Bi<sub>2</sub>Al<sub>4</sub>O<sub>9</sub> nanorods and RGO nanosheets on the piezoelectric properties of the composites.<sup>87</sup> X-ray diffraction (XRD) and Fourier-transform infrared (FTIR) spectroscopy showed that the  $\beta$ -phase content of PVDF increases from 53 to 76% with the addition of these nanofillers, as shown in Fig. 7. Through the working mechanisms of different composites, it has been found that the increase in piezoelectric properties is mainly attributed to the surface charge of Bi<sub>2</sub>Al<sub>4</sub>O<sub>9</sub>, which has a good interaction with the CH<sub>2</sub>- and CF<sub>2</sub>- dipoles of PVDF. In addition, the RGO nanosheets provide a conductive path for more charge to move to the electrode surface. When the applied electric field is 165 kV/cm, the residual polarization of the Bi<sub>2</sub>Al<sub>4</sub>O<sub>9</sub>/RGO/PVDF nanocomposite reaches 0.0189 mC/cm<sup>2</sup>, and the output voltage and current of the piezoelectric nanogenerator prepared by a Bi<sub>2</sub>Al<sub>4</sub>O<sub>9</sub>/RGO/PVDF nanocomposite are 5.92 V and 0.76 mA, respectively.

Kumar et al. prepared CNFs/PVDF composite nanofibers by electrospinning.<sup>88</sup> The synergistic effect of CNFs and subsequent electrical polarization steps could improve the piezoelectric properties of composite nanofibers by more than 5 times. Compared with other composite nanofibers, the CNFs/PVDF sample with 0.5 wt% CNFs exhibited a maximum voltage of  $5.80 \pm 0.17$  V and a short-circuit current of  $1.2 \pm 0.1$   $\mu$ A. Moreover, the carbon-based material CB has a very large surface area and plays a role in promoting  $\beta$ -nucleation in the preparation of P(VDF-HFP)-based composites,<sup>89</sup> it can significantly increase the  $\beta$ -phase content of P(VDF-HFP) and thus improve the piezoelectric properties of P(VDF-HFP). Hu et al. added two kinds of CB#300 and CB#3350 into P(VDF-HFP) by double-helical

**Table II** Properties of P(VDF-HFP) composites doped with different shapes and concentrations of ZnO.<sup>80</sup>

ZnO	Concentration (wt%)	Crystallinity (%)	Electroactivity	Elasticity (GPa)
–	0	46.21	0.34	$1.89 \pm 0.30$
NPs	1	46.21	0.47	$2.66 \pm 0.60$
	2	46.38	0.54	$2.68 \pm 0.67$
	3	46.02	0.49	$1.80 \pm 0.25$
NRs	1	46.09	0.49	$3.24 \pm 0.36$
	2	46.26	0.51	$3.36 \pm 0.39$
	3	46.23	0.49	$2.57 \pm 0.33$
MRs	1	47.58	0.48	$3.16 \pm 0.32$
	2	47.98	0.43	$4.43 \pm 0.70$
	3	48.04	0.39	$3.42 \pm 0.41$

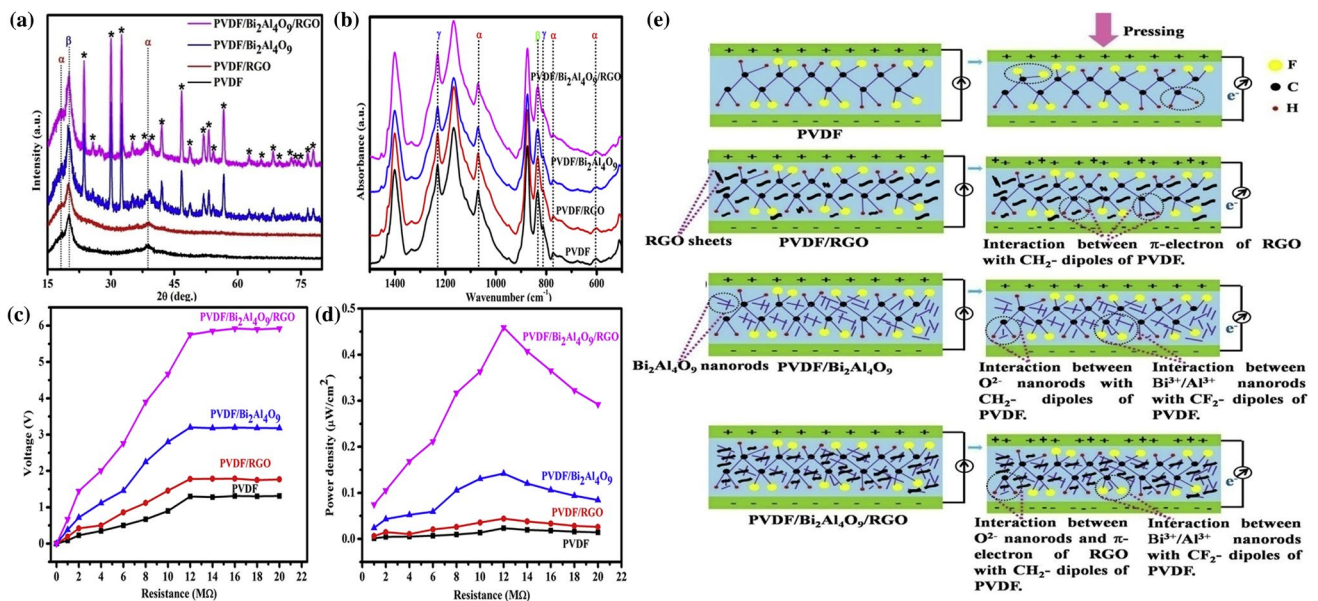


**Fig. 7** (a) XRD pattern and (b) FTIR of PVDF, PVDF/RGO, PVDF/Bi<sub>2</sub>Al<sub>4</sub>O<sub>9</sub>, and PVDF/Bi<sub>2</sub>Al<sub>4</sub>O<sub>9</sub>/RGO nanocomposite films. (c) Output voltage and (d) output power density of the nanocomposite films as a function of different load resistance (range 0~20 MΩ). (e) Work-

ing mechanism of PVDF, PVDF/RGO, PVDF/Bi<sub>2</sub>Al<sub>4</sub>O<sub>9</sub>, and PVDF/Bi<sub>2</sub>Al<sub>4</sub>O<sub>9</sub>/RGO nanocomposite films. (Adapted with permission from Ref. 87, copyright Elsevier).

melt-blending to improve its piezoelectric properties.<sup>90</sup> They found that the piezoelectric values of the composite film containing 0.5 wt% CB#3350 were 204%, 464%(AC), and 561%(DC), and the samples containing 0.5 wt% CB#300 were 211%, 475%(AC), and 624%(DC) higher than those of pure P(VDF-HFP) film.

## Metal Particles

Metal particles are also one of the functional fillers commonly used to enhance the piezoelectric properties of PVDF-based composites, where the doped particles are commonly Cu, Li, Fe, Pt, and Ag.<sup>91,92</sup> This is because the metal particles in the polymer matrix can be used as a  $\beta$ -build nuclear agent, which is helpful in raising the content of the electro-active phase. Jin et al. prepared ZnO/PVDF composites doped with Co, Na, Ag, and Li by spin-coating, and investigated their output voltages.<sup>93</sup> Under the same experimental conditions, Li-ZnO/PVDF devices produce peak voltage of the maximum 3.43 V, about 9 times of pure ZnO device, 1.2 times of Co-ZnO, 4.9 times of Na-ZnO, and 5.4 times of Ag-ZnO, respectively. In addition, the composite with doping ratio of 5 wt% shows a maximum output voltage. Moreover, by using an in-situ generation to Ghosh et al. compounds Pt nanoparticles and P(VDF-HFP) and prepares a nanocomposite film.<sup>94</sup> After that a new type of efficient ferroelectric nanogenerator (FTNG) based on the composite film was designed, which exhibited a good piezoelectric energy harvesting capability and a large

piezoelectric charge coefficient of -698 pC/N was obtained. They also found, under the compression normal stress of 4 MPa, FTNG has an open-circuit output voltage of about 18 V, a short-circuit current of 17.7 mA, and a high energy conversion efficiency (0.2%), respectively. In addition, Chen et al. prepared P(VDF-TrFE) based composites by vacuum solvent evaporation using Ag NPs and silver nanowires (Ag NWs) nanoparticles with different morphology as nanofillers.<sup>95</sup> It indicates that a decreasing of diameter of Ag NWs or an increasing of concentration of Ag NWs will improve the piezoelectric properties, leading to a high piezoelectric response by more than 3 times than that of pure P(VDF-TrFE) film.

## Other Fillers

In addition to the piezoelectric ceramics, carbon-based materials, and metal particles as functional fillers listed above, many other fillers, including cellulose nanocrystalline (CNC),<sup>96</sup> clay mineral sepiolite,<sup>97</sup> nano-clay (silicate aluminate),<sup>98</sup> nickel ferrite (NiFe<sub>2</sub>O<sub>4</sub>),<sup>99</sup> hydrated metal salts,<sup>100</sup> the rare earth element, Ce,<sup>101</sup> boron nitriding nanotubes (BNNTs), and two-dimensional materials of MXene can usually be used to fabricate the piezoelectric properties of polymer-based piezoelectric composites.<sup>17</sup> The mechanism is that the addition of these filler particles can induce the formation of  $\beta$ -phase crystals in the composite film, which is similar to other fillers. Taking Mxene as an example, Kim et al. demonstrated self-powered piezoelectric eskins with

a high sensitivity and broad sensing range based on 3D porous structures of MXene ( $\text{Ti}_3\text{C}_2\text{Tx}$ )/PVDF.<sup>102</sup> MXene ( $\text{Ti}_3\text{C}_2\text{Tx}$ ) has abundant surface functional groups, including oxide (=O), hydroxyl (-OH), and fluorine (-F). These can induce intermolecular hydrogen bonding with the  $\text{CH}_2$  groups of PVDF, which would result in the intercalation and confinement of PVDF between MXene nanosheets and the crystallization of polar  $\beta$ -phase PVDF (Fig. 8a). The formation of crystalline phases of PVDF was verified by XRD, FTIR, and x-ray photoelectron spectroscopy (XPS) analyses (Fig. 8b–d). These figures indicate that the interaction of the surface functional groups of MXene with the  $\text{CH}_2$  groups of PVDF promotes the formation of the  $\beta$  phase.

Therefore, when the functional filler is a composite with the polymer matrix, different polymer and functional fillers have different effects on the piezoelectric properties of the composites. For pure PVDF matrix, the doping effect of piezoelectric ceramic fillers is significant, since the piezoelectric property of traditional piezoelectric ceramic is larger than that of other fillers. However, no matter which filler is selected, the added amount should not be too large, so as not to exceed the compatibility value between the matrix and the filler interface, because defects will be introduced into the composite material, leading to

a considerable dielectric loss. Moreover, if P(VDF-HFP) is used as the matrix of the piezoelectric composites, their piezoelectric properties are significantly improved when P(VDF-HFP) is doped with metal particle fillers. The addition of metal particles can effectively promote the formation of the active phase of the piezoelectric  $\beta$ -phase in the composite material, thus effectively improving the piezoelectric properties of the material.

Especially, in P(VDF-TrFE)-based composites, the self-powered and wearable electronic devices based on P(VDF-TrFE)/BN NTs nanocomposites have the advantages of good piezoelectric output performance and shielding of neutron radiation, which can be applied in extreme space environments. In addition, RGO is also a filler that can significantly improve the piezoelectric properties. The interaction between RGO and the P(VDF-TrFE) matrix helps to break the central symmetry of the RGO, thereby enhancing the piezoelectric, ferroelectric, and triboelectric properties of P(VDF-TrFE)-based composite films. However, due to some limitations,<sup>103</sup> such as the low Curie temperature ( $T_c$ ) of 80–110 °C, reduced dipole density (defects caused by TrFE elements), insufficient raw material sources, and high cost, the use of P(VDF-TrFE) as a popular matrix on piezoelectric devices is restricted.

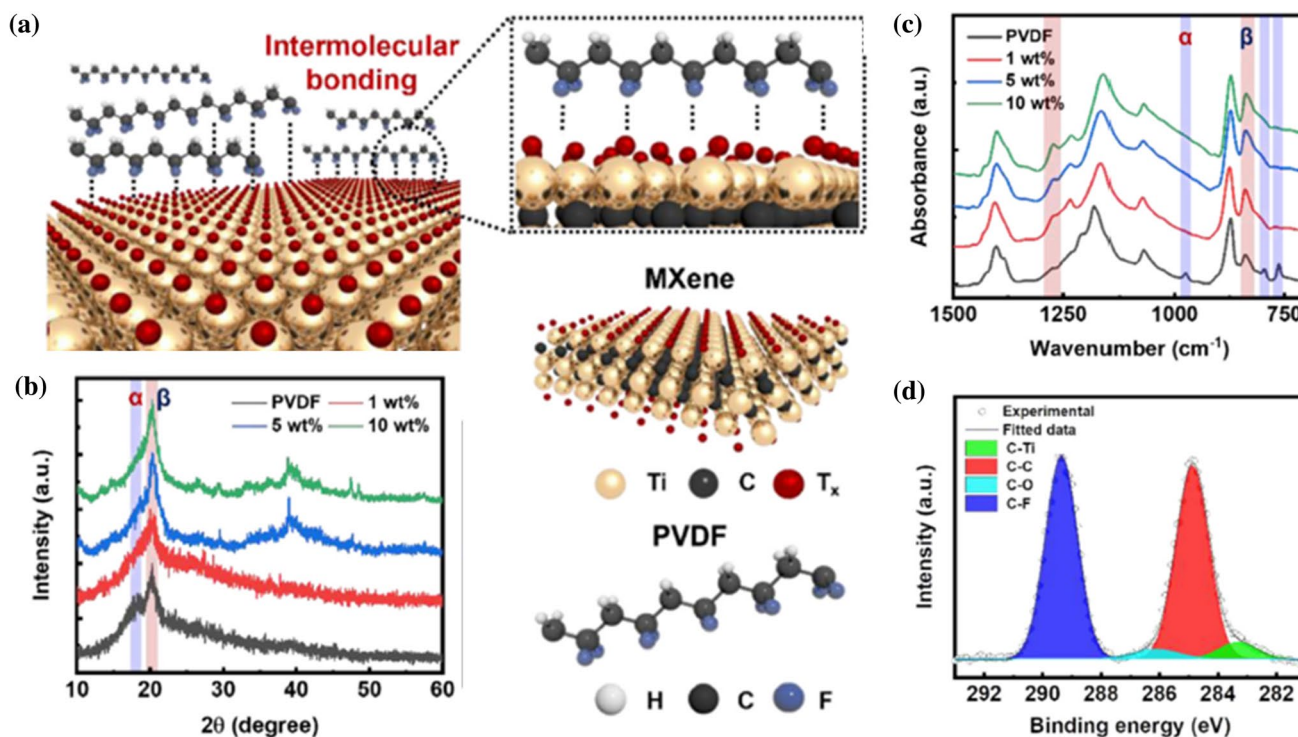


**Fig. 8** (a) Schematic of the interior structure formed by intermolecular hydrogen-bonding between PVDF and MXene, and the significantly enhanced formation of the polar  $\beta$ -phase. (b) XRD patterns and (c) FTIR analysis of PVDF and MXene/PVDF composites with dif-

ferent MXene concentrations. (d) XPS spectrum of the C1 s region of 10 wt% MXene/PVDF e-skin. (Adapted with permission from Ref. 102, copyright Elsevier).

## Prospect of Applications of PVDF-Based Piezoelectric Composites

Energy-harvesting devices mainly utilize the positive piezoelectric effect of piezoelectric materials to harvest and convert mechanical vibration energy in the environment into electric energy, thus providing energy for the working of micro-electronic components.<sup>104</sup> PVDF and its copolymer-based piezoelectric composites have attracted much attention because of their ease of manufacture and excellent flexible and piezoelectric properties. However, when piezoelectric composites are used as functional layers of flexible electronic devices, their low energy conversion efficiency seriously limits their further commercial applications. Therefore, it is difficult to obtain excellent performances of self-powered electronic devices solely by material optimization. It is still a challenge to improve the piezoelectric output and conversion performance of piezoelectric composites in piezoelectric electronic devices by optimizing their intrinsic structure design.<sup>105</sup> In this section, we will first introduce the application of self-powered electronic devices based on flexible polymer PVDF and its copolymer-based piezoelectric composites in the field of energy collection and conversion. The main research progress of piezoelectric nanogenerators and piezoelectric sensors is systematically summarized. The influence of different structure design on the piezoelectric output and sensing performance of flexible self-powered electronic devices is discussed. Finally, the challenges facing flexible self-powered electronic devices are proposed.

### Piezoelectric Nanogenerators

Piezoelectric nanogenerators are a kind of device that uses the piezoelectric effect of materials to convert mechanical energy into electrical energy. Under the action of external machinery, the polarization charge and the time-varying electric field generated by piezoelectric materials can drive the electrons to flow in an external circuit. Due to the advantages of small size, simple fabrication process, long working cycle, good stability, and environmental friendliness, piezoelectric generation based on piezoelectric composite materials is a promising method to realize the self-supply of electronic devices.<sup>106,107</sup>

Wang Zhonglin et al. first proposed the concept of energy harvesting in 2012, based on human motion, and designed a simple, practical, and durable flexible ZnO/PVDF plane/fiber piezoelectric nanogenerator, which has an ability to convert low-frequency (1 Hz) physical activity into electrical energy at different deformations. In addition, piezoelectric ceramics, such as KNN and BT,

are often selected as ceramic fillers.<sup>18,108–110</sup> Kang et al. further dispersed KNN nanoparticles into P(VDF-TrFE) nanofibers, which could effectively improve the piezoelectric energy-harvesting characteristics of the nanogenerators.<sup>111,112</sup> They found that the output voltage and current of the composite nanogenerator were 10 vol% KNN are 0.98 V and 78 nA, respectively. Moreover, Guo et al. designed and fabricated a flexible piezoelectric nanogenerator based on a modified BT nanoparticle MBT/P(VDF-TrFE) composite material, in which the BT is modified by 2-phosphobutane-1, 2, 4-tricarboxylic acid.<sup>113</sup> Compared with the generator with the BT NPs without modification, the MBT NP-doped nanogenerator possessed improved output performance of piezoelectric, as shown in Fig. 9. The main reason is that, after the modification of MBT NPs with organic phosphonic acid reactive groups, can make a strong inorganic nanopowder and polymer matrix interaction, and make MBT NPs in P(VDF-TrFE) disperse uniformly in the matrix and introduce fewer defects.

When ZnO is added to P(VDF-TrFE) matrix,<sup>114,115</sup> not only the piezoelectric properties of the two can be integrated but ZnO can also act as a nucleating agent to promote further crystallization of the polymer matrix, so that the piezoelectric property can be better improved. Li et al. modified ZnO NPs by adding dispersant (*n*-propylamine, PA) and silane coupling agent (1H, 2H, 1H, 2H, perfluorooctyltriethylsilane, PFOES).<sup>116</sup> Then, modified ZnO NPs was added into the P(VDF-TrFE) matrix as filler, forming a P(VDF-TrFE)-based composite film with high crystallinity, which was used as the functional layer of a piezoelectric nanogenerator. The piezoelectric strain constant of P(VDF-TrFE)/ZnO@PA@PFOES (P-Z-P-P) thin film is 73.5% higher than that of pure P(VDF-TrFE) film, and the output voltage of ITO/P-Z-P-P/Au PENG is 24.4% higher than that of ITO/P(VDF-TrFE)/Au PENG.

In addition to the piezoelectric nanogenerators based on the piezoelectric composite material prepared by the ZnO-doped polymer, other researchers have attempted to choose the metal oxides SnO<sub>2</sub> and MnO<sub>2</sub> as functional fillers to add to polymer matrix PVDF for the fabrication of piezoelectric nanogenerators.<sup>117</sup> Zhao et al. prepared MnO<sub>2</sub>/PVDF nanocomposites by electrospinning, hot-pressing and a rolling three-step method, and then designed and manufactured a piezoelectric nanogenerator based on MnO<sub>2</sub>/PVDF nanocomposites.<sup>118</sup> The addition of MnO<sub>2</sub> significantly improved the mechanical properties of the nanocomposites, and slightly increased their dielectric constants, which is conducive to the enhancement of piezoelectric output. When the content of MnO<sub>2</sub> is 1.0 wt%, the  $d_{33}$  is ~38 pC/N and the corresponding piezoelectric output response of the composite film reaches its peak value.

Polymer-based piezoelectric composites prepared by carbon-based multi-walled carbon nanotubes (MWCNTs),

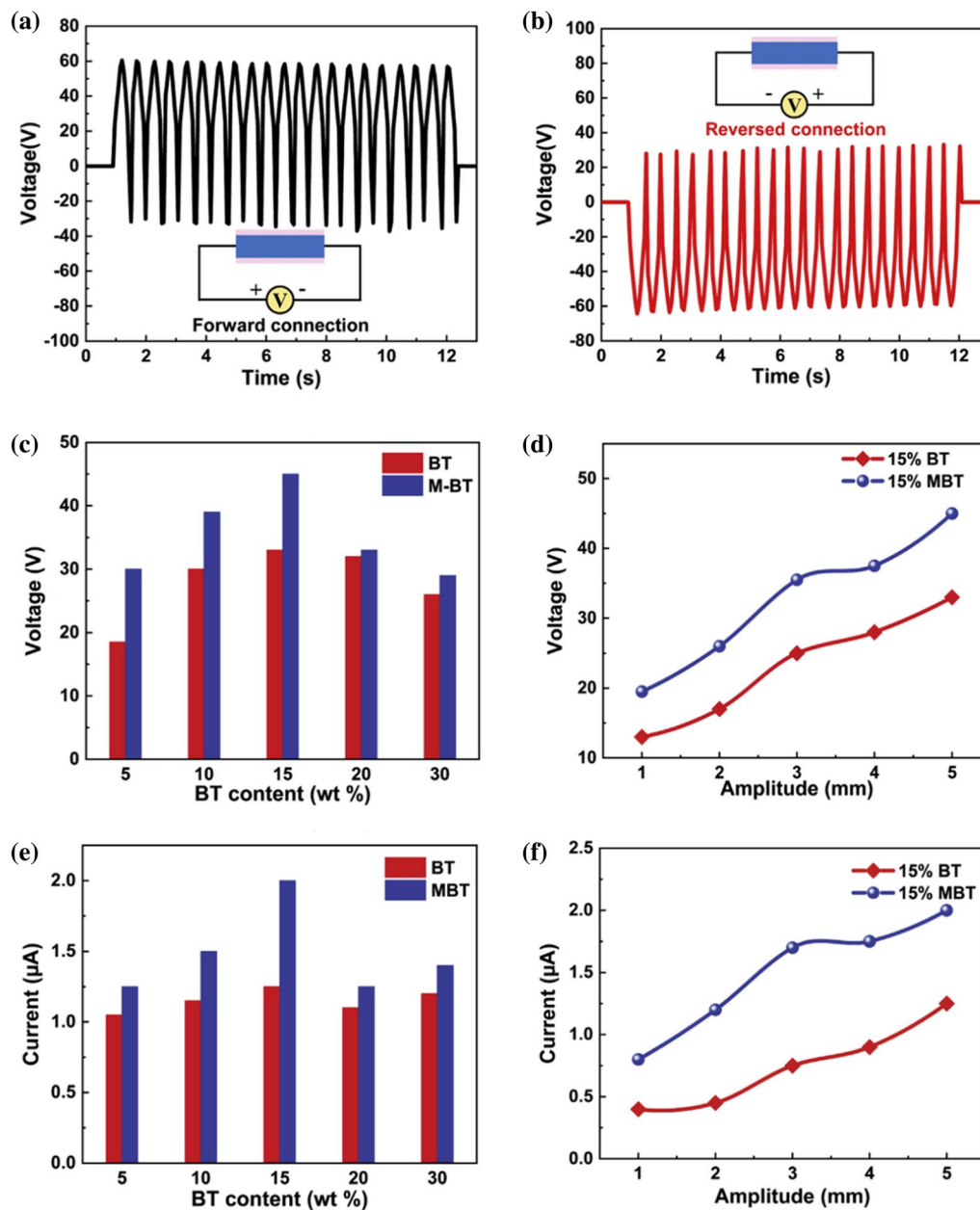


**Fig. 9** Output voltage of MBT nanogenerator in (a) forward direction and (b) reversed direction. Output voltage of (c) BT and MBT with different content, (d) 15 wt% BT and 15 wt% MBT with differ-

ent amplitudes. Output current of (e) BT and MBT with different BT content, (f) 15 wt% BT and 15 wt% MBT with different amplitudes. (Adapted with permission from Ref. 113, copyright Elsevier).

RGO, and the polymer P(VDF-TrFE) are also an effective way to fabricate piezoelectric nanogenerators with excellent performance.<sup>119</sup> Zhao et al. prepared flexible MWCNTs/P(VDF-TrFE) composite fiber thin films by electrospinning.<sup>120</sup> It was found that, when the MWCNTs content was 3 wt%, the electromechanical output voltage of the piezoelectric nanogenerator peaked at 18.23 V and the current was 2.14 A. In the load resistance of 10 M $\Omega$  and a frequency of 1 Hz strain for 20% of the test conditions, the output power density was 6.53  $\mu\text{W}/\text{cm}^2$ .

Moreover, a lead-free, simple, and low-cost RGO/P(VDF-TrFE) nanocomposite was prepared, and then was used as the raw material for a PENG and hybrid piezoelectric frictional electric nanogenerator (HPTENG) equipment.<sup>121</sup> The structural analysis of the material showed that the interaction between the RGO and the P(VDF-TrFE) matrix was helpful in breaking the central symmetry of RGO, thus enhancing the piezoelectric, ferroelectric, and triboelectric properties of the composite on the original P(VDF-TrFE) film. The piezoelectric output voltage of the

composite PENG device was 22 times higher than that of the pure P(VDF-TrFE)-based PENG. When the RGO content was 0.5 wt%, the maximum output voltage was 89.7 V. In addition, the average  $V_{oc}$  emission of composite thin film-based HPTENG devices was 227 V, which was much higher than that of pure P(VDF-TrFE)-based HPTENG.

In order to explore more new fillers used to enhance the piezoelectric properties, many researchers have chosen the metal ion salt ( $Zn^{2+}$ ,  $Eu^{3+}$ ),<sup>122,123</sup> zinc ferrite (ZF-R) moisture absorption of the rare earth salt, ytterbium,<sup>124,125</sup> in which half as many cage poly siloxane (POSS), polar additive  $BiCl_3$ , etc., can also play a role in the effect of piezoelectric properties of piezoelectric composite reinforced polymer matrixes. Liu et al. prepared POSS/P(VDF-TrFE) piezoelectric nanocomposites containing 0, 3, 5, and 8 wt% POSS by low-temperature solvent evaporation and thermal polarization.<sup>126</sup> The results show that POSS, as a kind of nanofiller, has good interfacial compatibility with P(VDF-TrFE) and does not affect the formation of  $\beta$ -phase in the P(VDF-TrFE) matrix. In addition, the average output voltage and current density of piezoelectric nanogenerators and friction nanogenerators were 3 V and  $0.5 \text{ mA/cm}^2$ , respectively, when the piezoelectric and friction nanogenerator designed and fabricated by composite materials were subjected to a force of 38 N over a  $1\text{-cm}^2$  area. A  $BiCl_3$ /PVDF nanofiber composite film was prepared by electrospinning through adding the polar additive  $BiCl_3$  into the PVDF matrix.<sup>127</sup> The output voltage of the piezoelectric nanogenerator based on a  $BiCl_3$ /PVDF composite membrane reached 1.1 V under the condition of vertical vibration, which was 4.76 times that of the pure

PVDF membrane piezoelectric nanogenerator, as shown in Fig. 10.

Although the performance of piezoelectric electronic devices can be improved to a certain extent by optimizing the materials, the main challenge of 0–3 piezoelectric composites is the poor stress conduction efficiency. That is, when the composite material is subjected to external forces, only a low level of stress is transferred to the piezoelectric functional layer, and most of the stress is wasted, which leads to poor piezoelectric conversion and output performance. In view of this challenge, many researchers are trying to prepare piezoelectric nanogenerators with excellent performance using both material selection and device structure design (Fig. 11). For example, Ye et al. synthesized a novel PENG based on P(VDF-TrFE)/BN NTs nanocomposite micropillar arrays with enhanced performance and excellent neutron radiation shielding using a reliable nano-imprint lithography.<sup>17</sup> These results demonstrated that a PENG based on the P(VDF-TrFE) micropillar array greatly enhanced the piezoelectric performance by a factor of 4.2 compared to pristine flat P(VDF-TrFE) film. By comparison, the introduction of BNNTs within the microstructured P(VDF-TrFE) film adds nearly another 2.6-fold enhancement, totaling an 11-fold enhancement. The high performances of PENGs based on P(VDF-TrFE)/BNNTs nanocomposite micropillar arrays are primarily ascribed to the synergistic effect due to flexible micropillar structure and high piezoelectric BNNTs nanofiller.<sup>128</sup>

Similarly, Chen et al. proposed a high-performance flexible piezoelectric nanogenerator based on a piezoelectrically-enhanced nanocomposite micropillar array of P(VDF-TrFE)/

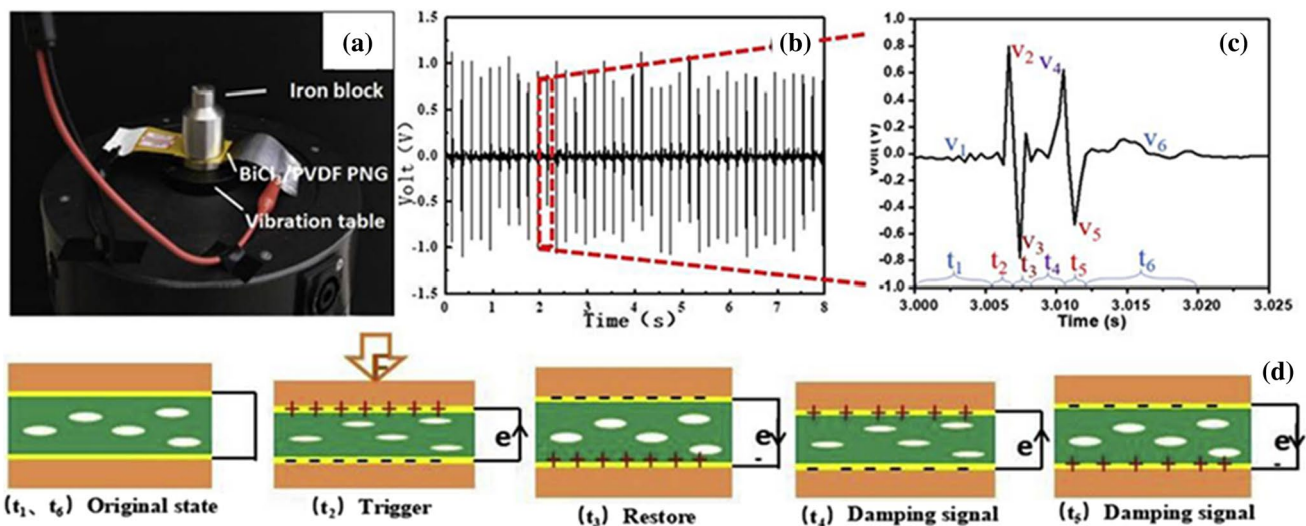


**Fig. 10** (a) Digital image of a  $BiCl_3$ /PVDF (2 wt%) piezoelectric nanogenerator attached to a vibrating table under a 150-g mass block, (b) the output voltage of the  $BiCl_3$ /PVDF (2 wt%) piezoelectric nanogenerator under continuous vibration with a frequency of 5 Hz and

an amplitude of 3 mm, (c) and (d) output voltage curve features and a schematic of the working mechanism during one vibration cycle, respectively. (Adapted with permission from Ref. 127, copyright Elsevier).

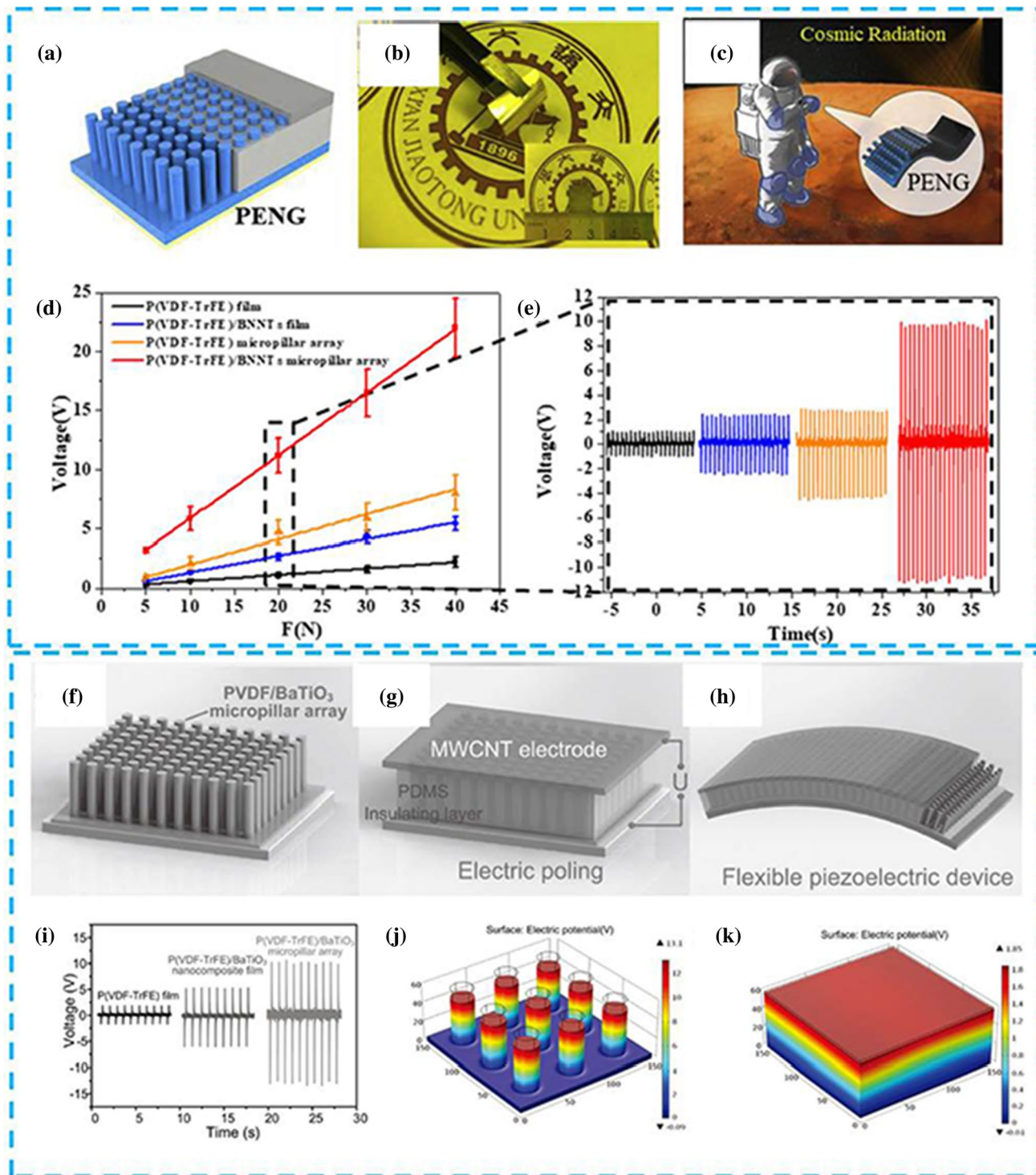


**Fig. 11** (a) Schematic representing the structure of a piezoelectric nanogenerator. (b) A flexible nanogenerator. (c) Schematic of the PENG's application for space energy harvesting. (d) The dependence of output voltage on applied forces for different piezoelectric nanogenerator based on bulk P(VDF-TrFE) film, bulk P(VDF-TrFE)/BNNTs nanocomposite film, P(VDF-TrFE) micropillar array, and P(VDF-TrFE)/BNNTs nanocomposite micropillar array. (e) Comparison of output voltages of four nanogenerators under 20 N applied force. (Adapted with permission from Ref. 17, copyright Elsevier). (f–h) Experimental methods for fabricating a high-performance

piezoelectric nanogenerator based on P(VDF-TrFE)/BaTiO<sub>3</sub> nanocomposite micropillar array. (i) A comparison of output voltages for piezoelectric devices based on a P(VDF-TrFE)/BaTiO<sub>3</sub> micropillar array, P(VDF-TrFE)/BaTiO<sub>3</sub> nanocomposite film, and for a bulk P(VDF-TrFE) film. (j, k) Simulation results of generated piezopotential distribution of two-unit blocks, (j) a unit micropillar array with a diameter of 22  $\mu\text{m}$  and a height of 55  $\mu\text{m}$ , the residual layer is 5  $\mu\text{m}$ , (k) a flat film unit with a thickness of 60  $\mu\text{m}$ . A constant external load of 5 mN was applied to simplify the simulation. (Adapted with permission from Ref. 129, copyright Wiley).

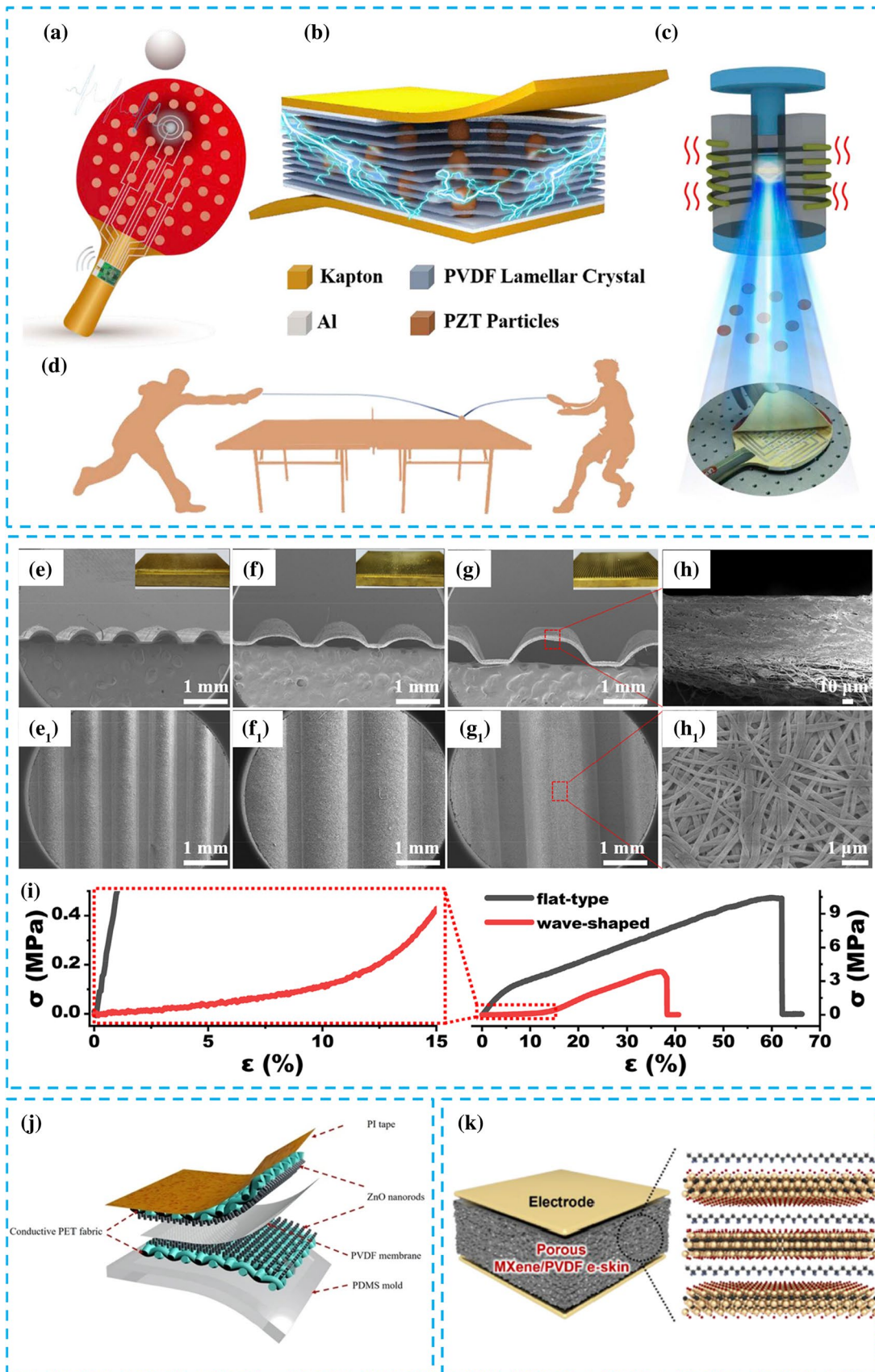




**Fig. 12** (a) Schematic of a smart racket for table tennis monitoring. (b) General illustration and detailed structure of the designed sensor. (c) The fabrication process of the piezocomposite and optical image of the smart racket. (d) The application of the smart table tennis racket. (Adapted with permission from Ref. 19, copyright Elsevier). SEM images of (e–h) cross-sectional and (e<sub>1</sub>–h<sub>1</sub>) surface morphologies of (e, e<sub>1</sub>) device 1, (f, f<sub>1</sub>) device 2 and (g, h, g<sub>1</sub>, h<sub>1</sub>) device 3. *Insets* in (e–g) are the copper templates used to fabricate the wave-shaped structures. (i) Tensile stress–strain curves of both flat-type and wave-shaped (device 3) fibrous membranes. (Adapted with permission from Ref. 137, copyright Springer Nature). (j) Schematic of the high-performance textile piezoelectric pressure sensor. (Adapted with permission from Ref. 138, copyright Springer Nature). (k) Schematic of porous MXene/PVDF e-skin and molecular structures of MXene and PVDF. (Adapted with permission from Ref. 102, copyright Elsevier).

BT for energy harvesting and highly sensitive self-powered sensing.<sup>129</sup> By a reliable and scalable nanoimprinting process, piezoelectrically-enhanced vertically aligned P(VDF-TrFE)/BT nanocomposite micropillar arrays were fabricated. The piezoelectric device exhibited an enhanced voltage of 13.2 V and a current density of 0.33  $\mu\text{A cm}^{-2}$ , which is an enhancement by a factor of 7.3 relative to pristine P(VDF-TrFE) bulk film. The mechanisms of high performance are mainly attributed to the enhanced piezoelectricity of the P(VDF-TrFE)/BT nanocomposite materials and the improved mechanical flexibility of the micropillar arrays.

## Piezoelectric Sensors

Piezoelectric sensors are based on the dielectric material piezoelectric effect of a sensor device. The so-called piezoelectric effect means that certain dielectric materials will produce deformation (compression, tensile deformation) when subjected to external forces in a certain direction, and that the polarization of internal charges will cause the surface of the dielectric material to become electrically charged. Piezoelectric sensors can convert the received pressure signal into an electrical signal, according to a certain conversion method, and have the advantages of simple structure, easy portability, wide frequency band, high sensitivity, and high operating stability. For example, wearable electronics have promising applications in physical and physiological monitoring, electronic skins (e-skins), and robotic sensing.<sup>102</sup> Flexible wearable pressure sensors have two important parts, namely elastic substrates that provide mechanical flexibility and sensitive materials that determine the sensing performance. As one of the most critical parameters, the sensitivity can be further improved by structural tuning of the sensitive material, affecting the fundamental performance of the sensor.

Recently, flexible piezoelectric sensors based on PVDF piezoelectric composite materials have been used to perceive the size of the surface reaction of flexible electronics,<sup>130,131</sup>

and they are commonly attached to a variety of irregular surfaces in the health, robotics, biomechanics, and other fields. Yang et al. modified a BT with polydopamine (PDA) as the surface modifier, and prepared PDA-BT/PVDF composite film by solution-casting.<sup>132</sup> The sensor based on 17 wt% PDA-BT/PVDF composite film exhibited a fast response of 61 ms and a piezoelectric output voltage of 9.3 V. In addition, as an energy supplier, even in the case of a high load resistance of 70 M $\Omega$ , the sensors could also produce a maximum power of 0.122 W/cm<sup>2</sup>. Such pressure sensors are believed to be sensitive to all kinds of human movements and show great potential in wearable electronics.

In addition to ceramic fillers, Lee et al. prepared a ZnO/PVDF composite film, and then designed a hybrid functional measurement sensor with high sensitivity, with the composite film as the piezoelectric functional layer and graphene as the electrode.<sup>133</sup> This sensor can simultaneously measure pressure and temperature in real time. The sensor uses piezoresistive changes in the piezoelectric functional layer to monitor pressure, and infers the temperature based on the signal recovery time. Thus, it can detect pressure changes of less than 10 Pa, three times lower than the minimum required for artificial skin, and temperature changes in the range of 20–120°C. Chen et al. prepared a new strain sensor based on a ZnO/P(VDF-TrFE) nanofiber composite by using electrospinning and hydrothermal processes,<sup>134</sup> which showed that the sensor had a fast response and recovery speed (0.4 s and 0.2 s, respectively), a high sensitivity (60% under 30% strain), a large strain coefficient (4.59), and a multifunctional sensing capability, including tensile deformation above 30% and bending deformation of up to 150%.

Moreover, carbon-based fillers are still used to enhance the piezoelectric properties of piezoelectric sensors, and P(VDF-TrFE)-based repolarized electrospinning composite film filled with modified RGO was proposed by electrospinning, and then a self-powered flexible pressure sensor was designed.<sup>135</sup> This showed that the piezoelectric output voltage and current of the repolarized composite film were up to 1.5 V and 0.125 A, respectively, and that the voltage is three times that of pure P(VDF-TrFE) film. Liu et al. designed a flexible sensing sensor based on electrospinning a MWCNTs/PVDF nanofiber array and an interdigital electrode.<sup>136</sup> This sensor could work under low-frequency environmental forces able to generate a peak voltage and current of 20.2 mV and 39 nA, respectively, under 6-Hz vibration condition, while the peak voltage of 24.4 mV and current of 130 nA were obtained at 15 Hz.

Piezoelectric sensors also have the same problems as piezoelectric nanogenerators, such as low stress transfer efficiency and poor piezoelectric output performance. To solve these problems, Yang Weiqing's team, starting from the device structure design, through the joint high-pressure nonsolvent-induced phase separation of two steps, prepared

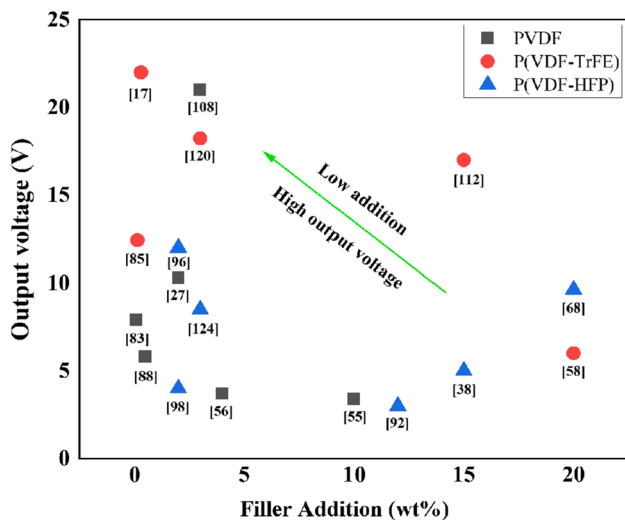


**Fig. 13** Comparison of output voltage of PVDF-based, P(VDF-HFP)-based, and P(VDF-TrFE)-based piezoelectric composite PENGs reinforced with various fillers.

a unique class of a wafer-structured puff pastry-shaped flexible PZT/PVDF piezoelectric composite sensor,<sup>19</sup> and successfully demonstrated its application in personalized table tennis training guidance. Using the unique structure of an interlayer potential accumulation effect and rapid stress release, the sensor shows excellent sensitivity (6.38 mV/N), ultra-fast response time (21 ms), and good mechanical stability (Fig. 12).

Similarly, a wavy PVDF nanofiber sensor has been fabricated.<sup>137</sup> The wavy PVDF nanofiber sensor achieves better longitudinal and transverse piezoelectric properties than planar devices, and can be applied to the detection and recognition of audible sound. In addition, a self-powered piezoelectric electronic skin based on MXene( $\text{Ti}_3\text{C}_2\text{Tx}$ )/PVDF 3D porous structure with high sensitivity and wide sensing range has been reported. The porous structure increases the contact area and local stress concentration in response to changes in applied pressure.<sup>102</sup> Tan et al. successfully designed a novel piezoelectric pressure sensor with flexible fabric based on ZnO nanorods.<sup>138</sup> Based on the above studies, it has been found that better piezoelectric performances can be achieved by the design of the device structures. For example, materials with a fully porous structure have higher compressibility (produce larger deformation) under the same pressure, and can also improve the sensitivity of the device.

Consequently, polymer-based piezoelectric composites are often used in piezoelectric nanogenerators, sensors, and other self-powered electronic components. Different compositions, designs, and manufacturing methods will significantly affect the piezoelectric output properties (output voltage and current) and performance parameters of piezoelectric devices.

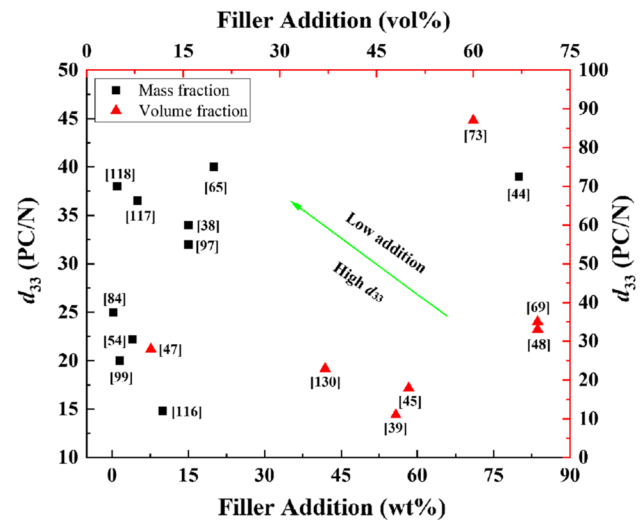


**Fig. 14** Comparison of  $d_{33}$  of PVDF-based and its copolymer-based piezoelectric composites reinforced with various fillers.

Figures 13 and 14 summarize the main piezoelectric output parameters and  $d_{33}$  of parts of different polymer-based composites doped with different fillers. Table III summarizes the performance parameters of different piezoelectric devices. To some extent, self-powered electronic devices based on polymer-based piezoelectric composites doped with different fillers can harvest various forms of mechanical energy in the environment and convert it into electrical energy for use, but there are still some shortcomings. PVDF-based and its copolymer-based composites have a good mechanical performance, high dielectric, and the advantages of high voltage. However, low interfacial compatibility between the filler and the polymer matrix will lead to the phenomenon of a separation of two phases, further influence the mechanical properties of materials, and reduce the service life of the device in practical application. In addition, for their power, electronic devices typically require rigid metal as the electrode layer,<sup>140</sup> which requires a good flexibility of the electronic equipment and corrosion resistance of the metal electrode layer. Therefore, it is expected that research and development of a fully flexible self-powered electronic device with polymer piezoelectric composite material as the piezoelectric layer and flexible material as the electrode layer will take place in the future.

## Summary and Perspective

At present, piezoelectric composite self-powered electronic devices based on PVDF and its copolymers have been widely studied for their excellent sensitivity, flexibility, durability, and compatibility with human skin. This paper firstly summarizes and analyzes the types of polymer matrix, functional

**Table III** Performance comparison of different composite-based self-powered electronic devices

Material	Input	Sensitivity	Response time	Recovery time	References
BNNTs/PVDF	0.4 MPa	55 V/MPa	–	–	17
PZT/PVDF	–	6.38 mV/N	21 ms	30 ms	19
BT/PVDF	1 MPa	35 V/MPa	–	–	62
PVDF/NaNbO <sub>3</sub> /RGO	15 kPa	–	195 ms	–	71
MXene/PVDF	< 2.5 kPa	11.9 nA/kPa	53 ms (20 kPa)	73 ms (20 kPa)	102
BT/P(VDF-TrFE)	5–60	257.9 mV/N	–	–	129
PZT/PVDF	2.125 N	86.580 mV/N	–	–	130
GO/BT/PVDF	80–230 kPa	10.89 ± 0.5 mV/kPa	–	–	131
PDA@BTO/PVDF	33 kPa	–	61 ms	–	132
ZnO/PVDF	0–2.25 kPa	0.62 V/kPa	–	–	138
Pt/PVDF	< 10 N	72 mV/N (< 10 N)	–	–	139

fillers, and preparation technology of polymer matrix piezoelectric composites, and then introduces the research progress of piezoelectric nanogenerators and piezoelectric sensors, two self-powered electronic devices, focusing on material selection and structural design. The piezoelectric properties of a single piezoelectric polymer can be improved by introducing a specific filler or selecting a suitable processing technology. In addition, the output and sensing performance of the device can be significantly enhanced by the design of the device structure. Although the conversion and output performance of piezoelectric composite-based electronic devices have made great progress, through the continuous optimization of materials and preparation process selection, device structure design, and other aspects, there are still many problems to be solved, and more work needs to be carried out in the following aspects to solve the key problems:

- (1) The interaction mechanism between substrate and filler in piezoelectric composites needs to be further studied. For example, since the electrical properties of composites depend to a large extent on the degree of polarization generated by the materials, the interface polarization is a major contributor to the total polarization of the composites. Therefore, more in-depth research is needed on the mechanism of action at the interface between the matrix and the filler.
- (2) For piezoelectric composites, the polymer matrix and the filler are not of the same material, the dispersion of the filler in the polymer matrix is poor, and the filler is easy to agglomerate in the matrix, leading to defects. Thus, how to optimize the preparation processes and compositions of the two different phases, and how to add appropriate modifiers and improve the dispersion of the filler in the matrix, is also an attractive area.
- (3) In addition, by developing new polymer-based piezoelectric composites for energy harvesting, researchers have designed and fabricated a number of self-powered

electronic devices that meet the needs of various fields. However, due to self-powered electronic devices generally requiring rigid metal electrode layers, the flexibility of the devices is limited, and the metal electrode layers are susceptible to corrosion. Therefore, it is expected that research and development of a fully flexible self-powered electronic device with polymer piezoelectric composite material as the piezoelectric layer and flexible material as the electrode layer will take place in the future.

In brief, although the current development of self-powered electronic devices based on flexible PVDF and its copolymer-based piezoelectric composites faces various challenges, flexible electronic devices are still the future development trend. With the successive proposals of new materials, new structures, and new preparation methods and their application in the design of flexible piezoelectric devices, it is believed that flexible piezoelectric nanogenerators and sensors that meet practical application requirements will be developed and designed in the near future.

**Acknowledgments** This work was supported in part by National Natural Science Foundation of China (NSFC 51773168 and 92066204), NSFC of Shaanxi province (2020JM-465), and by the Shaanxi project of Education Department (21JY031).

**Conflict of interest** The authors declare that they have no conflict of interest.

## References

1. X.L. Chen, H.M. Tian, X.M. Li, J.Y. Shao, Y.C. Ding, N.L. An, and Y.P. Zhou, *Nanoscale* 7, 11536 (2015).
2. C. Ribeiro, V. Sencadas, J.L.G. Ribelles, and S. Lanceros-Mendez, *Soft Mater.* 8, 274 (2010).
3. J. Scheinbeim, *J. Appl. Phys.* 50, 4399 (1979).
4. D. Vatansever, R.L. Hadimani, T. Shah, and E. Siores, *Smart Mater. Struct.* 20, 055019 (2011).

5. P. Martins, A.C. Lopes, and S. Lanceros-Mendez, *Prog. Polym. Sci.* 39, 683 (2014).
6. A. Salimi and A.A. Yousefi, *J. Polym. Sci. Pol. Phys.* 42, 3487 (2004).
7. E. Kar, N. Bose, S. Das, N. Mukherjee, and S. Mukherjee, *Phys. Chem. Chem. Phys.* 17, 22784 (2015).
8. P. Sukwisute, N. Muensit, S. Soontaranon, and S. Rugmai, *Appl. Phys. Lett.* 103, 063905 (2013).
9. X.H. Liu, S.Y. Liu, M.G. Han, L. Zhao, H.M. Deng, J. Li, Y.M. Zhu, K.E. Lia, and S.O. Brien, *Nanoscale Res. Lett.* 8, 374 (2013).
10. M. Rahimabady, K. Yao, S. Arabnejad, L. Lu, V.P.W. Shim, and D.C.W. Chet, *Appl. Phys. Lett.* 100, 252907 (2012).
11. P. Adhikary, S. Garain, and D. Mandal, *Phys. Chem. Chem. Phys.* 17, 7275 (2015).
12. J. Nunes-Pereira, P. Martins, V.F. Cardoso, C.M. Costa, and S. Lanceros-Mendez, *Mater. Design* 104, 183 (2016).
13. N. Jia, Q. He, J. Sun, G.M. Xia, and R. Song, *Polym. Test.* 57, 302 (2017).
14. C.Y. Wan and C.R. Bowen, *J. Mater. Chem. A* 5, 3091 (2017).
15. X.P. Hu, S.H. Yu, and B.J. Chu, *Mater. Design* 192, 108700 (2020).
16. M. Venkatesan, W.C. Chen, C.J. Cho, L. Veeramuthu, L.G. Chen, K.Y. Li, M.L. Tsai, Y.C. Lai, W.Y. Lee, W.C. Chen, and C.C. Kuo, *Chem. Eng. J.* 433, 133620 (2022).
17. S.B. Ye, C. Cheng, X.M. Chen, X.L. Chen, J.Y. Shao, J. Zhang, H.W. Hu, H.M. Tian, X.M. Li, L. Ma, and W.B. Jia, *Nano Energy* 60, 701 (2019).
18. B. Dudem, D.H. Kim, L.K. Bharat, and J.S. Yu, *Appl. Energ.* 230, 865 (2018).
19. G. Tian, W.L. Deng, Y.Y. Gao, D. Xiong, C. Yan, X.B. He, T. Yang, L. Jin, X. Chu, and H.T. Zhang, *Nano Energy* 59, 574 (2019).
20. C.Y. Tang, X. Zhao, J. Jia, S. Wang, X.J. Zha, B. Yin, K. Ke, R.Y. Bao, Z.Y. Liu, Y. Wang, K. Zhang, M.B. Yang, and W. Yang, *Nano Energy* 90, 106603 (2021).
21. Y.J. Yang, S. Aziz, S.M. Mehdi, M. Sajid, S. Jagadeesan, and K.H. Choi, *J. Electron. Mater.* 46, 4172 (2017).
22. M.F. Lin, J.Q. Xiong, J.X. Wang, K. Parida, and P.S. Lee, *Nano Energy* 44, 248 (2018).
23. Z.M. Huang, Y.Z. Zhang, M. Kotaki, and S. Ramakrishna, *Compos. Sci. Technol.* 63, 2223 (2003).
24. S.W. Choi, J.R. Kim, Y.R. Ahn, S.M. Jo, and E.J. Cairns, *Chem. Mater.* 19, 104 (2007).
25. E. Fukada and T. Sakurai, *Polym. J.* 2, 656 (1971).
26. C.H. Lang, J. Fang, H. Shao, X. Ding, and T. Lin, *Nat. Commun.* 7, 11108 (2016).
27. Y. Li, M.H. Xu, Y.S. Xia, J.M. Wu, X.K. Sun, S. Wang, G.H. Hu, and C.X. Xiong, *Chem. Eng. J.* 388, 124205 (2020).
28. X.H. Hu, Y.G. Jiang, Z.Q. Ma, Q.P. He, Y.P. He, T.F. Zhou, D.Y. Zhang, and A.C.S. Appl. *Polym. Mater.* 2, 4399 (2020).
29. S. Divya, and J. Hemalatha, *Eur. Polym. J.* 88, 136 (2017).
30. B. Mahale, D. Bodas, S.A. Gangal, and B. Mater, *Sci.* 40, 569 (2017).
31. T. Nishiyama, T. Sumihara, E. Sato, and H. Horibe, *Polym. J.* 49, 319 (2017).
32. V.F. Cardoso, C.M. Costa, G. Minas, and S. Lanceros-Mendez, *Smart Mater. Struct.* 21, 85020 (2012).
33. U. Yaqoob, R.M. Habibur, M. Sheeraz, and H.C. Kim, *Compos. Part B-Eng.* 159, 259 (2019).
34. P.H. Hu, L.L. Yan, C.X. Zhao, Y.Y. Zhang, and J. Niu, *Compos. Sci. Technol.* 168, 327 (2018).
35. Y. Cho, J.B. Park, B.S. Kim, J. Lee, W.K. Hong, I.K. Park, J.E. Jang, J.I. Sohn, S. Cha, and J.M. Kim, *Nano Energy* 16, 524 (2015).
36. X.M. Cai, T.P. Lei, D.H. Sun, and L.W. Lin, *RSC Adv.* 7, 15382 (2017).
37. P. Singh, H. Borkar, B.P. Singh, V.N. Singh, and A. Kumar, *AIP Adv.* 4, 087117 (2014).
38. Y. Ma, W.S. Tong, W.J. Wang, Q. An, and Y.H. Zhang, *Compos. Sci. Technol.* 168, 397 (2018).
39. M. Wegener, and K. Arlt, *J. Phys. D Appl. Phys.* 41, 165409 (2008).
40. Z.H. Liu, C.T. Pan, L.W. Lin, J.C. Huang, and Z.Y. Ou, *Smart Mater. Struct.* 23, 025003 (2014).
41. A. Salimi and A.A. Yousefi, *Polym. Test.* 22, 699 (2003).
42. B. Satish, K. Sridevi, and M.S. Vijaya, *J. Phys. D Appl. Phys.* 35, 2048 (2002).
43. S.P. Muduli, S. Parida, S.K. Rout, S. Rajput, and M. Kar, *Mater. Res. Express* 6, 095306 (2019).
44. K. Yu, S. Hu, W.D. Yu, and J.Q. Tan, *J. Electron. Mater.* 48, 2329 (2019).
45. J.Z. Pei, Z.H. Zhao, X.Q. Li, H.J. Liu, and R. Li, *Mater. Express* 7, 180 (2017).
46. J. Fu, Y.D. Hou, X. Gao, M.P. Zheng, and M.K. Zhu, *Nano Energy* 52, 391 (2018).
47. R.X. Xu, W. Chen, J. Zhou, Y.M. Li, and H.J. Sun, *J. Wuhan Univ. Technol.* 21, 84 (2006).
48. J.H. Seol, J.S. Lee, H.N. Ji, Y.P. Ok, G.P. Kong, K.S. Kim, C.Y. Kim, and W.P. Tai, *Ceram. Int.* 38, S263 (2011).
49. D.J. Shin, J.H. Ji, J. Kim, G.H. Jo, S.J. Jeong, and J.H. Koh, *J. Alloy. Compd.* 802, 562 (2019).
50. A. Patra, A. Pal, and S. Sen, *Ceram. Int.* 44, 11196 (2018).
51. L. Yang, M. Cheng, W.Y. Lyu, M.X. Shen, J.H. Qiu, H.L. Ji, and Q.Y. Zhao, *Compos. Part A-Appl. S.* 107, 536 (2018).
52. L. Yang, Q.Y. Zhao, K.N. Chen, Y.Z. Ma, Y.P. Wu, H.L. Ji, J.H. Qiu, and A.C.S. Appl. *Mater. Inter.* 12, 11045 (2020).
53. M. Kim, Y.S. Wu, E.C. Kan, and J. Fan, *Polymers* 10, 745 (2018).
54. F.A. He, K. Lin, D.L. Shi, H.J. Wu, H.K. Huang, J.J. Chen, F. Chen, and K.H. Lam, *Compos. Sci. Technol.* 137, 138 (2016).
55. S. Bairagi and S.W. Ali, *Org. Electron.* 78, 105547 (2020).
56. S. Bairagi and S.W. Ali, *Eur. Polym. J.* 116, 554 (2019).
57. X.J. Zhao, W. Zhang, S.J. Chen, J. Zhang, and X.L. Wang, *J. Polym. Res.* 19, 9862 (2012).
58. X.R. Zhou, K. Parida, O. Halevi, Y.Z. Liu, J.Q. Xiong, S. Magdassi, and P.S. Lee, *Nano Energy* 72, 104676 (2020).
59. X.Y. Guan, B.G. Xu, and J.L. Gong, *Nano Energy* 70, 104516 (2020).
60. C. Zhang, H.J. Sun, and Q.Y. Zhu, *J. Electron. Mater.* 50, 6426 (2021).
61. S.H. Wankhade, S. Tiwari, A. Gaur, and P. Maiti, *Energy Rep.* 6, 358 (2020).
62. Y.L. Zhao, Q.L. Liao, G.J. Zhang, Z. Zhang, Q.J. Liang, X.Q. Liao, and Y. Zhang, *Nano Energy* 11, 719 (2015).
63. S. Siddiqui, D.I. Kim, L.T. Duy, M.T. Nguyen, S. Muhammad, W.S. Yoon, and N.E. Lee, *Nano Energy* 15, 177 (2015).
64. Y. Rao, J.M. Qu, T. Marinis, C.P. Wong, and I.E.E.E.T. Compon, *Pack. T.* 23, 680 (2000).
65. L. Yang, Q.Y. Zhao, Y. Hou, L.Y. Hong, H.L. Ji, L. Xu, K.J. Zhu, M.X. Shen, H.J. Huang, H.Y. He, and J.H. Qiu, *Compos. Sci. Technol.* 174, 33 (2019).
66. I.Y. Abdullah, M. Yahaya, M.H.H. Jumali, and H.M. Shanshool, *Opt. Quant. Electron.* 48, 149 (2016).
67. J. Nunes-Pereira, V. Sencadas, V. Correia, V.F. Cardoso, W.H. Han, J.G. Rocha, and S. Lanceros-Mendez, *Compos. Part B-Eng.* 72, 130 (2015).
68. S.H. Lee, Y.C. Choi, M.S. Kim, K.M. Ryu, and Y.G. Jeong, *Fiber. Polym.* 21, 473 (2020).
69. B. Ponraj, R. Bhimireddi, and K.B.R. Varma, *J. Adv. Ceram.* 5, 308 (2016).

70. S. An, H.S. Jo, G. Li, E. Samuel, S.S. Yoon, and A.L. Yarin, *Adv. Funct. Mater.* 30, 2001150 (2020).
71. H.H. Singh, S. Singh, and N. Khare, *Compos. Sci. Technol.* 149, 127 (2017).
72. J. Kang, P.S. Xie, Y. Li, J.L. Zhu, and L. Li, *Appl. Mech. Mater.* 487, 58 (2014).
73. Y.J. Choi, M.J. Yoo, H.W. Kang, H.G. Lee, S.H. Han, and S. Nahm, *J. Electroceram.* 30, 30 (2013).
74. J.S. Dodds, F.N. Meyers, and K.J. Loh, *IEEE Sens. J.* 12, 1889 (2012).
75. D.E. Motaung, G.H. Mhlongo, S.S. Nkosi, G.Y. Malgas, B. Mwakikunga, E. Coetsee, H.C. Swart, H.M.I. Abdallah, T. Moyo, S.S. Ray, and A.C.S. Appl. Mater. Inter. 6, 8981 (2014).
76. Z. Yang, Z.Z. Ye, Z. Xu, and B.H. Zhao, *Physica E* 42, 116 (2009).
77. X.D. Li, Y. Chen, A. Kumar, A. Mahmoud, J.A. Nychka, H.J. Chung, and A.C.S. Appl. Mater. Inter. 7, 20753 (2015).
78. Z.L. Wang and J.H. Song, *Science* 312, 242 (2006).
79. R.S. Sabry, and A.D. Hussein, *Polym. Test.* 79, 106001 (2019).
80. K. Phooptub, and N. Muensit, *Micro Nano Lett.* 13, 1063 (2018).
81. S.C. Karumuthil, S.P. Rajeev, S. Varghese, and A.C.S. Appl. Nano. Mater. 2, 4350 (2019).
82. J.C. Shu, and M.S. Cao, *Surf. Tech.* 49, 29 (2020).
83. M.M. Abolhasani, K. Shirvanimoghaddam, and M. Naebe, *Compos. Sci. Technol.* 138, 49 (2017).
84. J. Lee and S. Lim, *J. Ind. Eng. Chem.* 67, 478 (2018).
85. L.K. Wu, M. Jing, Y.L. Liu, H.M. Ning, X.Y. Liu, S.F. Liu, L.Y. Lin, N. Hu, and L.B. Liu, *Compos. Part B-Eng.* 164, 703 (2019).
86. S.H. Bae, O. Kahya, B.K. Sharma, J. Kwon, H.J. Cho, B. Ozyilmaz, and J.H. Ahn, *ACS Nano* 7, 3130 (2013).
87. A. Anand, D. Meena, and M.C. Bhatnagar, *J. Alloy. Compd.* 843, 156019 (2020).
88. R.S. Kumar, T. Sarathi, K.K. Venkataraman, and A. Bhattacharyya, *Mater. Lett.* 255, 126515 (2019).
89. J. Cai, N. Hu, L.K. Wu, Y.H. Liu, Y. Li, H.M. Ning, X.Y. Liu, and L.Y. Lin, *Compos. Part A-Appl. S.* 121, 223 (2019).
90. B. Hu, N. Hu, L.K. Wu, H. Cui, and J. Ying, *Funct. Mater. Lett.* 8, 1540006 (2015).
91. R. Sahoo, S. Mishra, L. Unnikrishnan, S. Mohanty, S. Mahapatra, S.K. Nayak, S. Anwar, and A. Ramadoss, *Mat. Sci. Semicon. Proc.* 117, 105173 (2020).
92. D. Mandal, K. Henkel, and D. Schmeisser, *Phys. Chem. Chem. Phys.* 16, 10403 (2014).
93. C.R. Jin, N.J. Hao, Z. Xu, I. Trase, Y. Nie, L. Dong, A. Closson, Z. Chen, and J.X.J. Zhang, *Sensor. Actuat. A-Phys.* 305, 111912 (2020).
94. S.K. Ghosh, T.K. Sinha, B. Mahanty, and D. Mandal, *Energy Technol.* 3, 1190 (2015).
95. H.J. Chen, S.J. Han, C. Liu, Z.H. Luo, H.P.D. Shieh, R.S. Hsiao, and B.R. Yang, *Sensor Actuat A-Phys.* 245, 135 (2016).
96. D. Ponnamma, H. Parangusan, A. Tanvir, and M.A. AlMa'adeed, *Mater. Design* 184, 108176 (2019).
97. S.J. Zhang, W.S. Tong, J. Wang, W.J. Wang, Z.H. Wang, and Y.H. Zhang, *J. Appl. Polym. Sci.* 137, 48412 (2020).
98. S. Tiwari, A. Gaur, C. Kumar, and P. Maiti, *Energy* 171, 485 (2019).
99. D. Ponnamma, O. Aljarod, H. Parangusan, and M.A. AlMaadeed, *Mater. Chem. Phys.* 239, 122257 (2020).
100. J. Yuennan, P. Sukwisute, and N. Muensit, *Mater. Res. Express* 5, 055702 (2018).
101. Y.Y. Zhuang, J.L. Li, Q.Y. Hu, S. Han, W.H. Liu, C. Peng, Z. Li, L. Zhang, X.Y. Wei, and Z. Xu, *Compos. Sci. Technol.* 200, 108386 (2020).
102. J. Kim, M. Jang, G. Jeong, S. Yu, J. Park, Y. Lee, S. Cho, J. Yeom, Y. Lee, A. Choe, Y.R. Kim, Y. Yoon, S.S. Lee, K.S. An, and H. Ko, *Nano Energy* 89, 106409 (2021).
103. K. Maity, S. Garain, K. Henkel, D. Schmeisser, D. Mandal, and A.C.S. Appl. Polym. Mater. 2, 862 (2020).
104. C. Colombo, L. Vergani, and M. Burman, *Compos. Struct.* 94, 1165 (2012).
105. M.Y. Yan, J.W. Zhong, S.W. Liu, Z.D. Xiao, X. Yuan, D. Zhai, K.C. Zhou, Z.Y. Li, D. Zhang, C. Bowen, and Y. Zhang, *Nano Energy* 88, 106278 (2021).
106. A.F. Arrieta, T. Delpero, A. Bergamini, and P. Ermanni, *Appl. Phys. Lett.* 102, 173904 (2013).
107. J. Nunes-Pereira, V. Sencadas, V. Correia, J.G. Rocha, and S. Lanceros-Mendez, *Sensor. Actuat. A-Phys.* 196, 55 (2013).
108. S. Bairagi and S.W. Ali, *Energy* 198, 117385 (2020).
109. K.M. Shi, B. Sun, X.Y. Huang, and P.K. Jiang, *Nano Energy* 52, 153 (2018).
110. S.H. Shin, Y.H. Kim, J.Y. Jung, M.H. Lee, and J. Nah, *Nanotechnology* 25, 485401 (2014).
111. H.B. Kang, C.S. Han, J.C. Pyun, W.H. Ryu, C.Y. Kang, and Y.S. Cho, *Compos. Sci. Technol.* 111, 1 (2015).
112. Z. Zhou, Z. Zhang, Q.L. Zhang, H. Yang, Y.L. Zhu, Y.Y. Wang, L. Chen, and A.C.S. Appl. Mater. Inter. 12, 1567 (2020).
113. H.L. Guo, Q. Wu, H.J. Sun, X.F. Liu, and H.T. Sui, *Mater. Today Energy* 17, 100489 (2020).
114. B. Mahanty, S.K. Ghosh, S. Garain, and D. Mandal, *Mater. Chem. Phys.* 186, 327 (2017).
115. P. Fakhri, B. Amini, R. Bagherzadeh, M. Kashfi, M. Latifi, N. Yavari, S.A. Kani, and L.X. Kong, *RSC Adv.* 9, 10117 (2019).
116. J. Li, C.M. Zhao, K. Xia, X. Liu, D. Li, and J. Han, *Appl. Surf. Sci.* 463, 626 (2019).
117. E. Kar, N. Bose, B. Dutta, S. Banerjee, N. Mukherjee, and S. Mukherjee, *Energy Convers Manage* 184, 600 (2019).
118. Q.Y. Zhao, L. Yang, K.N. Chen, Y.Z. Ma, Q.R. Peng, H.L. Ji, and J.H. Qiu, *Compos. Sci. Technol.* 199, 108330 (2020).
119. R.M. Habibur, U. Yaqoob, S. Muhammad, A.S.M.I. Uddin, and H.C. Kim, *Mater. Chem. Phys.* 215, 46 (2018).
120. C.X. Zhao, J. Niu, Y.Y. Zhang, C. Li, and P.H. Hu, *Compos. Part B-Eng.* 178, 107447 (2019).
121. R. Bhunia, S. Gupta, B. Fatma, Prateek, R.K. Gupta, and A. Garg, *ACS Appl. Mater. Inter.*, 11, 38177 (2019).
122. P. Adhikary, and D. Mandal, *Phys. Chem. Chem. Phys.* 19, 17789 (2017).
123. P. Adhikary, S. Garain, S. Ram, and D. Mandal, *J. Polym. Sci. Polym. Phys.* 54, 2335 (2016).
124. I. Chinya, A. Pal, and S. Sen, *Mater. Res. Bull.* 118, 110515 (2019).
125. S.K. Ghosh, A. Biswas, S. Sen, C. Das, K. Henkel, D. Schmeissere, and D. Mandal, *Nano Energy* 30, 621 (2016).
126. Y.Z. Liu, H. Zhang, J.X. Yu, Z.Y. Huang, C. Wang, and Y. Sun, *RSC Adv.* 10, 17377 (2020).
127. C. Chen, Z.K. Bai, Y.Z. Cao, M.C. Dong, K.K. Jiang, Y.S. Zhou, Y.Z. Tao, S.J. Gu, J. Xu, X.Z. Yin, and W.L. Xu, *Compos. Sci. Technol.* 192, 108100 (2020).
128. S.M. Nakhmanson, A. Calzolari, V. Meunier, J. Bernholc, and M. Buongiorno-Nardelli, *Phys. Rev. B* 67, 235406 (2003).
129. X.L. Chen, X.M. Li, J.Y. Shao, N.L. An, H.M. Tian, C. Wang, T.Y. Han, L. Wang, and B.H. Lu, *Small* 13, 1604245 (2017).
130. N. Chamankar, R. Khajavi, A.A. Yousefi, A. Rashidi, and F. Golestanifard, *Ceram. Int.* 46, 19669 (2020).
131. M.M. Zhu, M.N. Lou, I. Abdalla, J.Y. Yu, Z.L. Li, and B. Ding, *Nano Energy* 69, 104429 (2020).
132. Y. Yang, H. Pan, G.Z. Xie, Y.D. Jiang, C.X. Chen, Y.J. Su, Y. Wang, and H.L. Tai, *Sensor. Actuat. A-Phys.* 301, 111789 (2020).
133. J.S. Lee, K.Y. Shin, O.J. Cheong, J.H. Kim, and J. Jang, *Sci. Rep.* 5, 7887 (2015).
134. S. Chen, Z. Lou, D. Chen, Z.J. Chen, K. Jiang, and G.Z. Shen, *Sci. China Mater.* 59, 173 (2016).

135. P. Li, L.B. Zhao, Z.D. Jiang, M.Z. Yu, Z. Li, and X.J. Li, *Macromol. Mater. Eng.* 304, 1900504 (2019).
136. Z.H. Liu, C.T. Pan, C.Y. Su, L.W. Lin, Y.J. Chen, and J.S. Tsai, *Sensor. Actuat. A-Phys.* 211, 78 (2014).
137. F. Xu, J. Yang, R.Z. Dong, H.X. Jiang, C.H. Wang, W.L. Liu, Z.X. Jiang, X.Q. Zhang, and G.D. Zhu, *Adv. Fiber Mater.* 3, 368 (2021).
138. Y.S. Tan, K. Yang, B. Wang, H. Li, L. Wang, and C.X. Wang, *Nano Res* 14, 3969 (2021).
139. S.K. Ghosh and D. Mandal, *Nano Energy* 53, 245 (2018).
140. M.M. Alam, S. Lee, M. Kim, K.S. Han, V.A. Cao, and J. Nah, *Nano Energy* 72, 104672 (2020).

**Publisher's Note** Springer Nature remains neutral with regard to jurisdictional claims in published maps and institutional affiliations.